REPORT 1155

A COMPARISON OF THE EXPERIMENTAL SUBSONIC PRESSURE DISTRIBUTIONS ABOUT SEVERAL BODIES OF REVOLUTION WITH PRESSURE DISTRIBUTIONS COMPUTED BY MEANS OF THE LINEARIZED THEORY [1]

By Clarence W. Matthews

SUMMARY

An analysis is made of the effects of compressibility on the pressure coefficients about several bodies of revolution by comparing experimentally determined pressure coefficients with corresponding pressure coefficients calculated by the use of the linearized equations of compressible flow. The results show that the theoretical methods predict the subsonic pressure-coefficient changes over the central part of the body but do not predict the pressure-coefficient changes near the nose. Extrapolation of the linearized subsonic theory into the mixed subsonic-supersonic flow region fails to predict a rearward movement of the negative pressure-coefficient peak which occurs after the critical stream Mach number has been attained. Two equations developed from a consideration of the subsonic compressible flow about a prolate spheroid are shown to predict, approximately, the change with Mach number of the subsonic pressure coefficients for regular bodies of revolution of fineness ratio 6 or greater.

INTRODUCTION

A number of papers have been published concerning the theoretical aspect of the effects of compressibility on the flow over bodies of revolution (refs. 1 to 4). In the present investigation these theoretical methods are applied to the analysis of experimental data. Such an analysis should contribute to the basic knowledge of subsonic three-dimensional flow.

Two prolate spheroids of fineness ratios 6 and 10, an ogival body, and a prolate spheroid with an annular bump near the nose were tested in this investigation. The experimental pressures about the two prolate spheroids are compared with the pressures computed by the linearized compressible-flow theory. Several relations developed from theoretical considerations of the flow about a prolate spheroid are presented for correcting the incompressible pressure coefficients of regular bodies of fineness ratios 6 to 10 for the effects of compressibility in the subcritical flow range. Results obtained from these relations are also compared with corresponding experimental pressure coefficients.

SYMBOLS

b	maximum radius of body
C_N	normal-force coefficient based on plan-form area of ellipse
f	fineness ratio of body, $l/2b$
l	total length of body (see fig. 1)
M_{cr}	critical Mach number
M_0	free-stream Mach number
p_l	local static pressure
p_0	free-stream static pressure
P	pressure coefficient, $\dfrac{p_l-p_0}{\frac{1}{2}\rho V^2}$
r	local radius of body
$S(x)$	cross-sectional area of body of revolution
u	component of local velocity parallel to free stream
U	free-stream velocity
v	component of local velocity in vertical plane perpendicular to free stream
V	total local velocity
w	component of local velocity perpendicular to u and v
x	coordinate along major axis of body
α	angle of attack
$\beta=\sqrt{1-M_0^2}$	
γ	ratio of specific heat at constant pressure to specific heat at constant volume
ρ	density
φ	velocity potential
μ, ζ, ω	ellipsoidal coordinates (see ref. 5)

Subscripts:

c	compressible value
i	incompressible value
cr	critical value
st	incompressible value of flow about hypothetical stretched body

MODELS

Sketches of the bodies of revolution tested, which show the locations of the pressure orifices and other pertinent details, are presented in figure 1. The ordinates of the typical transonic or ogival body and the prolate spheroid with an annular bump are given in table I. The ordinates of the section of the sting support, which is a part of the body of revolution, are those of a prolate spheroid of fineness ratio 6. The same support was used for each body. The couplings used to change the angle of attack were mounted in the sting 11 inches downstream from the end of the body.
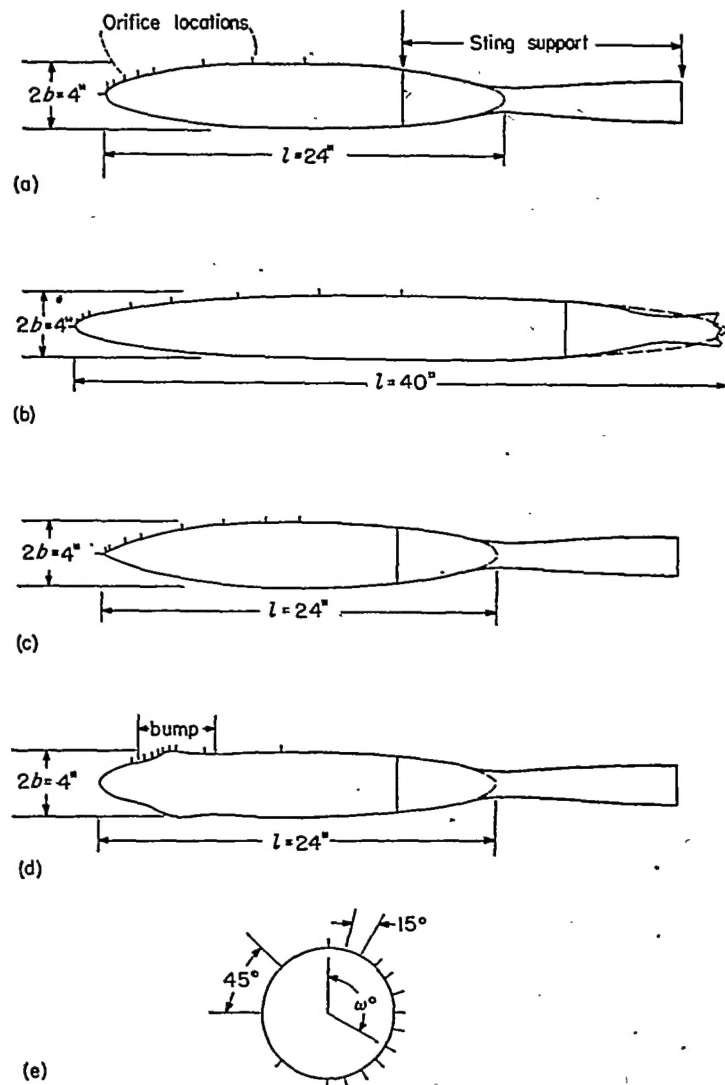
(a) Prolate spheroid; $f=6$.
(b) Prolate spheroid; $f=10$.
(c) Typical transonic body.
(d) Prolate spheroid with annular bump.
(e) Angular locations of orifices.

FIGURE 1.—Profiles of bodies tested.

Except at the first three stations indicated in figures 1 (a) to 1 (d), the pressure orifices were located around the body as shown in figure 1 (e). These orifices were spaced 15° apart on one side of the body in order to obtain a fairly accurate normal-force coefficient upon integration of the pressure coefficients. The orifice at the first station was located in the nose. The orifices at the next two stations were located at 90° intervals around the body. The pressure orifice openings were 0.010 inch in diameter.

TESTS

The pressures about the bodies were measured in the Langley 8-foot high-speed tunnel through the Mach number range 0.3 to 0.95. The angle-of-attack ranges were 0° to 7.7° for the regular bodies and 0° to 2° for the prolate spheroid with an annular bump. The pressures were recorded by photographing a 10-foot 100-tube manometer board filled with acetylene tetrabromide.

TABLE I.—ORDINATES OF THE TYPICAL TRANSONIC BODY AND OF THE ANNULAR BUMP PROLATE SPHEROID

Transonic body		Prolate spheroid with annular bump	
x/l, percent	r/l, percent	x/l, percent	r/l, percent
0.00	0.000	0.00	0.000
.50	.462	.75	1.437
.75	.596	1.25	1.854
1.25	.854	2.50	2.604
2.50	1.445	5.00	3.631
5.00	2.409	10.00	5.000
10.00	3.940	12.50	5.560
20.00	6.180	12.91	5.684
30.00	7.480	13.33	5.873
40.00	8.121	14.16	6.408
50.00	8.333	15.20	7.230
60.00	8.162	16.24	7.800
70.00	7.635	17.49	8.190
75.00	7.215	17.91	8.230
		18.74	8.250
		20.00	8.230
		23.32	8.220
		25.00	8.000
		27.08	7.810
		28.31	7.663
		28.74	7.620
		29.16	7.605
		30.00	7.640
		35.00	7.952
		50.00	8.290
		55.00	8.333
		65.00	8.290
		75.00	7.952

The free-stream pressures and Mach numbers were determined from an empty-tunnel calibration based on the pressures at an orifice located 4 feet upstream of the model.

Several preliminary plots of local pressure coefficients as functions of free-stream Mach number showed considerable scatter for Mach numbers less than 0.5, probably because of the difficulty of reading the small pressure differences and because of the possibility that the tunnel was not held at each Mach number a sufficient length of time to insure complete settling of the manometer liquid. Because of this scatter, it was necessary to neglect the pressure coefficients below $M_0=0.5$ in extrapolating the pressure-coefficient curves to a stream Mach number of zero. The data used in the analysis in this investigation were picked from the extrapolated curves.

For the tests reported herein, the Reynolds number varies from approximately 2,700,000 per foot at $M_0=0.40$ to 3,950,000 at $M_0=0.94$.

The wall interference may be approximately determined by using the equations of reference 6. Since the corrections were small, they were not applied to the pressures in the figures which present experimental data alone; however, the corrections, even though small, were applied to the experimental data used for the comparisons between the theoretical and the experimental values.

THEORETICAL METHODS

The theoretical subsonic pressures about a prolate spheroid may be computed by applying the Prandtl-Glauert correction to the incompressible potential-flow equations in the manner suggested in reference 7. In this solution of the linearized form of the equations for compressible flow, the body is stretched in the free-stream direction by the factor $1/\beta$; the induced velocity components $u-U$, v, and w about the stretched body are computed by potential-flow methods (for prolate spheroids, see ref. 5); and the induced velocities $u-U$, v, and w are corrected by the factors $1/\beta^2$, $1/\beta$, and $1/\beta$,

respectively. The corrected velocities are the compressible velocities at the corresponding points on the original body. The following formula, as is shown in appendix A, is the result of the application of this method to the flow over prolate spheroids:

$$1-\frac{V^2}{U^2}=\frac{1}{\beta^2}\left\{1-\frac{H_{st}^2}{G_{st}}-K_{b_{st}}^2\sin^2\omega\sin^2\alpha_{st}\right.$$
$$-\left(\frac{1}{\beta^2}-1\right)\left[\left(1-\frac{H_{st}F_{st}}{G_{st}}\right)^2\right.$$
$$+\left(K_{b_{st}}\sin^2\omega\sin^2\alpha_{st}+\frac{H_{st}F_{st}}{G_{st}}\right)^2$$
$$\left.\left.-\left(\frac{H_{st}F_{st}}{G_{st}}\right)^2-2K_{b_{st}}\sin^2\omega\sin^2\alpha_{st}\right]\right\} \tag{1}$$

where

$$F_{st}=\sqrt{1-\mu^2}\cos\alpha_{st}-\mu\sqrt{1-e_{st}^2}\cos\omega\sin\alpha_{st}$$

$$G_{st}=1-e_{st}^2\mu^2$$

$$H_{st}=\sqrt{1-\mu^2}K_{a_{st}}\cos\alpha_{st}-\mu\sqrt{1-e_{st}^2}K_{b_{st}}\cos\omega\sin\alpha_{st}$$

$$K_{a_{st}}=1-\frac{\left(\log\frac{1+e_{st}}{1-e_{st}}\right)-2e_{st}}{\left(\log\frac{1+e_{st}}{1-e_{st}}\right)-\frac{2e_{st}}{1-e_{st}^2}}$$

$$K_{b_{st}}=1-\frac{\left(\log\frac{1+e_{st}}{1-e_{st}}\right)-\frac{2e_{st}}{1-e_{st}^2}}{\left(\log\frac{1+e_{st}}{1-e_{st}}\right)-\frac{2e_{st}(1-2e_{st}^2)}{1-e_{st}^2}}$$

$$e_{st}=\sqrt{1-\frac{\beta^2}{f^2}}$$

$$\tan\alpha_{st}=\beta\tan\alpha$$

The pressure coefficients may be computed from the following relation:

$$P_c=\frac{\left[1+\frac{\gamma-1}{2}M_0^2\left(1-\frac{V^2}{U^2}\right)\right]^{\frac{\gamma}{\gamma-1}}-1}{\frac{\gamma}{2}M_0^2} \tag{2}$$

Because of the nature of the transformation, equation (1) does not hold for large angles of attack (that is, where $\alpha=\sin\alpha$ ceases to be a fair approximation) or for bodies of small fineness ratio.

The compressibility effects indicated by application of the linearized theory of compressible flow to prolate spheroids are not apparent from equations (1) and (2). The effects may be shown simply for the special case of the center of a prolate spheroid at zero angle of attack. As shown in appendix B, the following relation is obtained:

$$\frac{P_c}{P_i}=\left(1+\frac{\log\beta}{1-\log 2f}\right)\left[\frac{f^2-\log 2f}{f^2-\beta^2(\log 2f-\log\beta)}\right] \tag{3}$$

Thus, the theoretical solution indicates that the ratio of the compressible pressure coefficient to the incompressible pressure coefficient on bodies of revolution will vary conformably

with a function of $\log\beta$ and f rather than with $1/\beta$ as in two-dimensional flow. Equation (3) may be reduced to the form $\frac{P_c}{P_i}=1+\frac{\log\beta}{1-\log 2f}$ which is presented in reference 8.

Another and easier method of obtaining an approximate solution of the linearized equations for very thin bodies may be found in references 2 to 4. This method consists of integrating an approximated source-sink distribution to obtain the induced-velocity ratios from which the pressure coefficients may be computed. Since the source-sink distribution is approximated by the derivative of the cross-sectional area with respect to the length of the body, this method is more generally applicable to bodies of revolution than is the method of applying the Prandtl-Glauert correction to the exact incompressible-flow solution. It is shown in appendix A that, for prolate spheroids at zero angle of attack, this method gives the following result:

$$P_c=\frac{1}{f^2}\left[\frac{1}{2\sqrt{\left(1-\frac{x}{l}\right)^2+\beta^2\frac{r^2}{l^2}}}+\frac{1}{2\sqrt{\frac{x^2}{l^2}+\beta^2\frac{r^2}{l^2}}}-\right.$$
$$\left.\log\frac{1-\frac{x}{l}+\sqrt{\left(1-\frac{x}{l}\right)^2+\beta^2\frac{r^2}{l^2}}}{-\frac{x}{l}+\sqrt{\frac{x^2}{l^2}+\beta^2\frac{r^2}{l^2}}}\right] \tag{4}$$

Two approximate forms which show the effects of compressibility can be obtained from equation (4) by considering (a) the difference, (P_c-P_i), and (b) the ratio P_c/P_i of the compressible and the incompressible values. These two relations may be reduced to the following forms when $\frac{\beta^2 r^2}{l^2}$ is considered small with respect to $\left(1-\frac{x}{l}\right)^2$ or $\frac{x^2}{l^2}$:

$$P_c-P_i=\frac{2\log\beta}{f^2} \tag{5}$$

$$\frac{P_c}{P_i}=1+\frac{\log\beta}{1-\log 2f} \tag{6}$$

Both relations indicate that the effect of compressibility on the subsonic flow about a body of revolution at any given Mach number is to lower the pressure coefficients over a large part of the body. These relations for the effect of compressibility are in accord with similar equations presented in references 2 and 3.

RESULTS AND ANALYSIS

COMPARISON OF EXPERIMENTAL AND THEORETICAL PRESSURE DISTRIBUTIONS

The local pressure-coefficient distributions are presented in figures 2 to 6 for various values of free-stream Mach number. Figures 7 to 9 are replots of some of the data of the preceding figures corrected for wall interference, together with results of the theoretical calculations by means of equations (2) and (4). Figures 2 to 6 show a decrease in the experimental pressures over the central part of the body with increasing Mach number, as predicted by equation (5).

However, figures 7 to 9 indicate that the linearized theory predicts a decrease in the pressures over the entire body, whereas the experimental data show that a point on the body exists ahead of which the pressures increase rather than decrease. (See also figs. 2 to 6.) The lack of agreement of the linearized theory with the experimental results near the nose of the body is to be expected because of the assumptions made in its derivation. It might be pointed out that the effect of compressibility on the experimental pressure coefficients is approximately to rotate the pressure-coefficient distributions about the point at which the incompressible pressure coefficient is zero. The actual point about which the rotation may be considered to take place shifts its location from slightly downstream of the stream-pressure point on the top of the body to slightly upstream of the stream-pressure point on the bottom of the body.

M_O	
○	0
◁	.300
□	.600
◇	.800
△	.900
▽	.920
▷	.940

Percent distance from nose, x/l
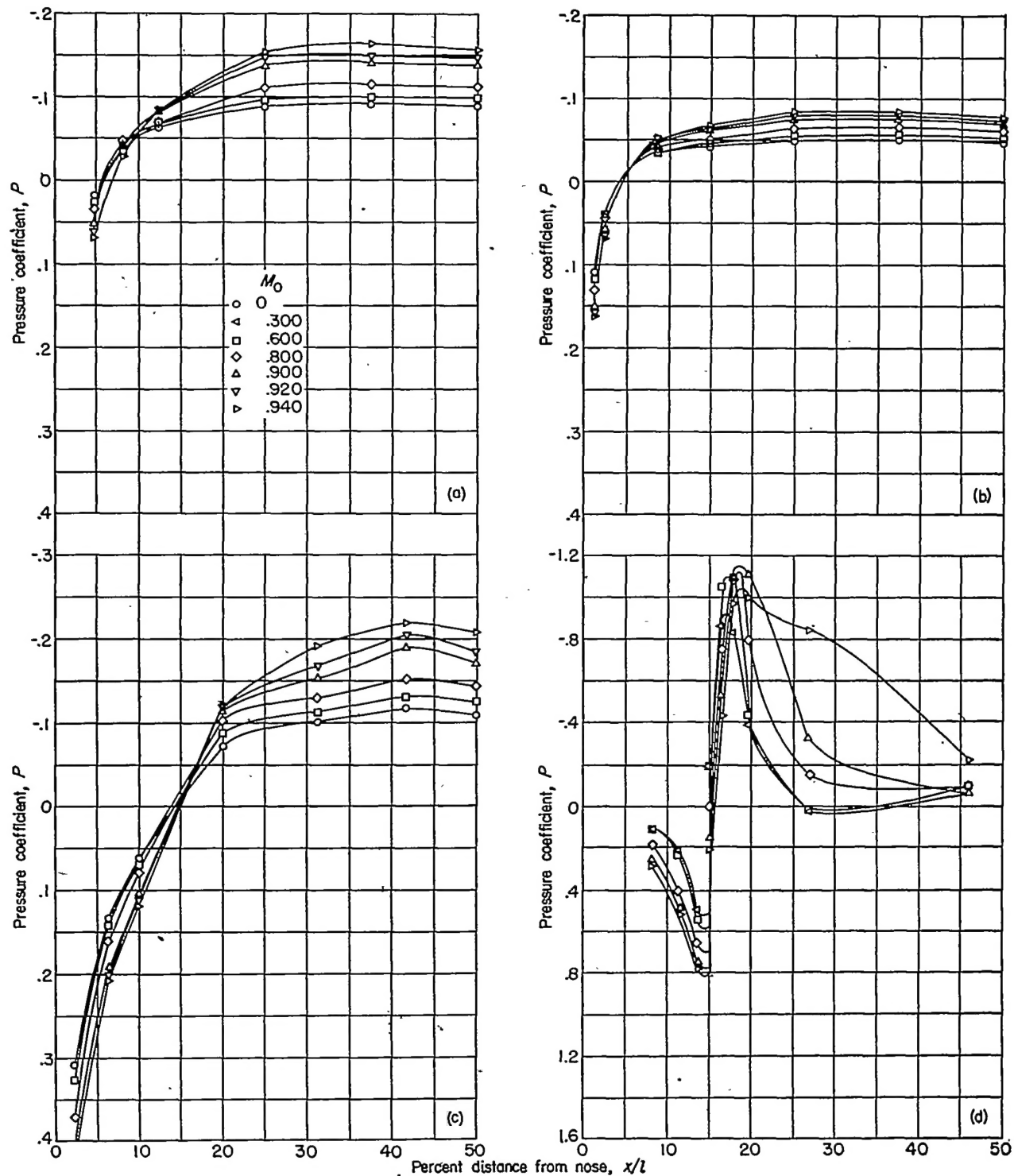
(a) Prolate spheroid; $f=6$; $M_{cr}=0.916$.
(c) Typical transonic body; $M_{cr}=0.898$.
(b) Prolate spheroid; $f=10$; $M_{cr}=0.947$.
(d) Prolate spheroid with annular bump; $M_{cr}=0.634$.

FIGURE 2.—Experimental pressure distributions over several bodies of revolution at zero angle of attack.

(a) $\omega = 0°$.
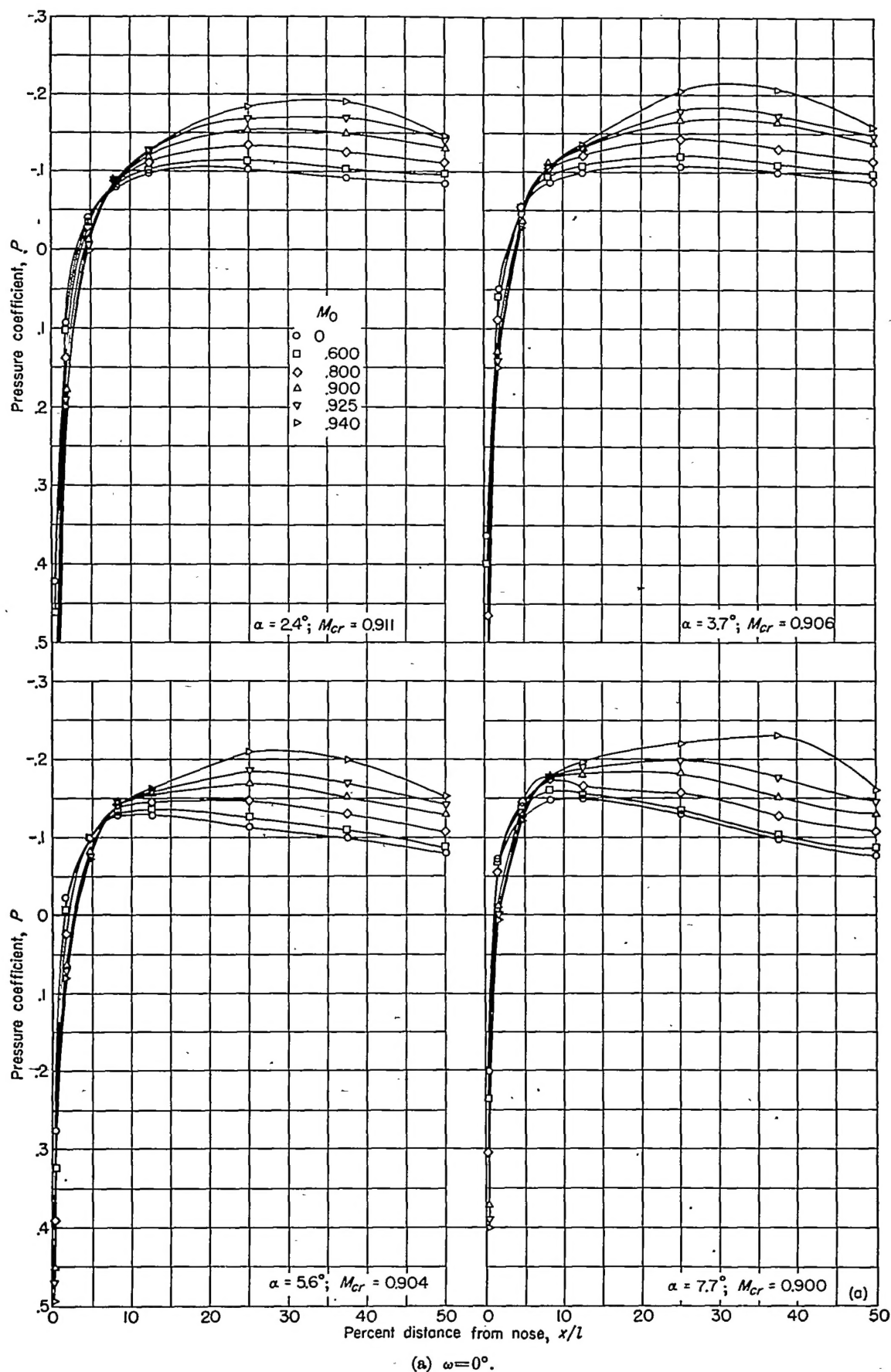
FIGURE 3.—Experimental pressure distributions over a prolate spheroid of fineness ratio 6 at several angles of attack.
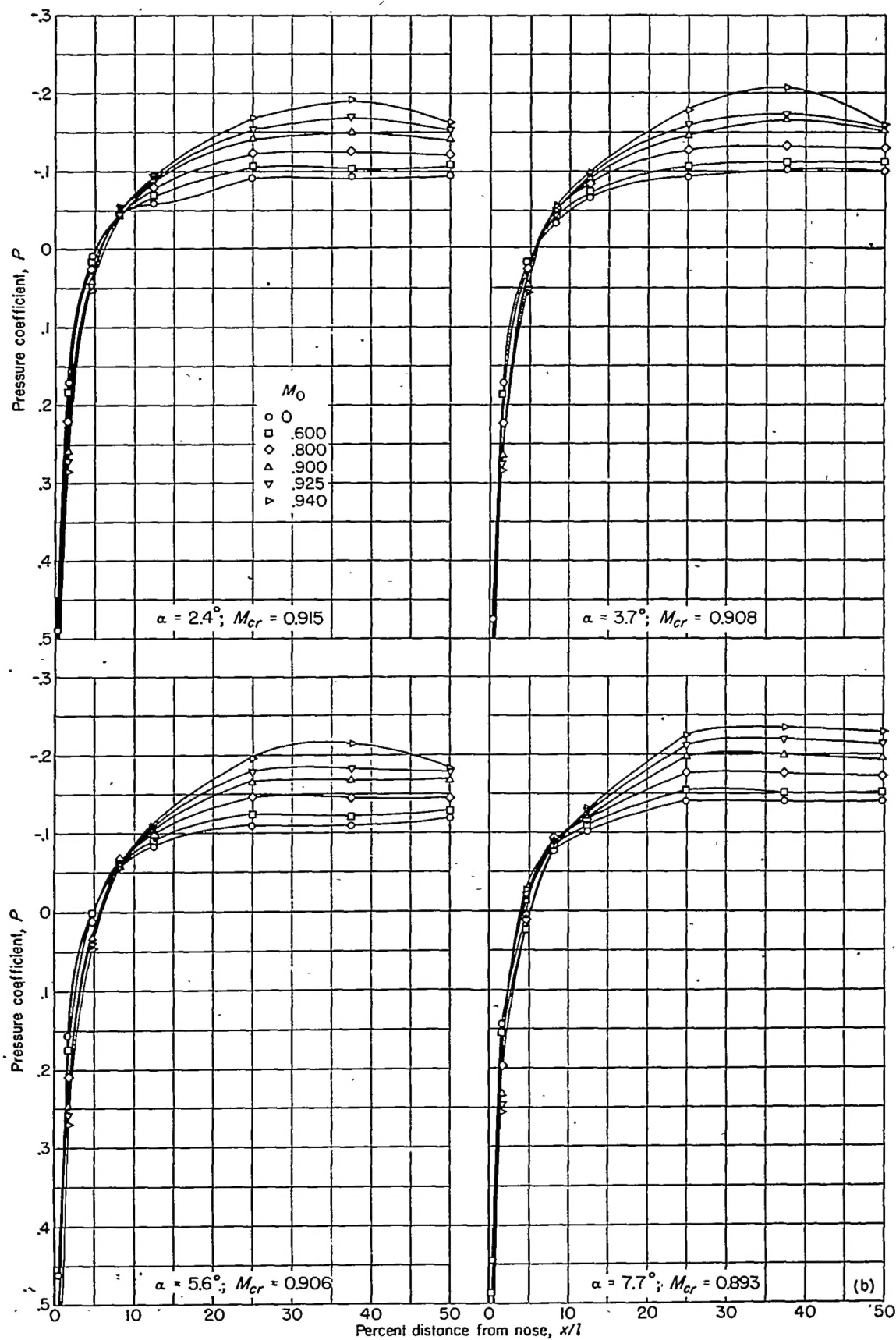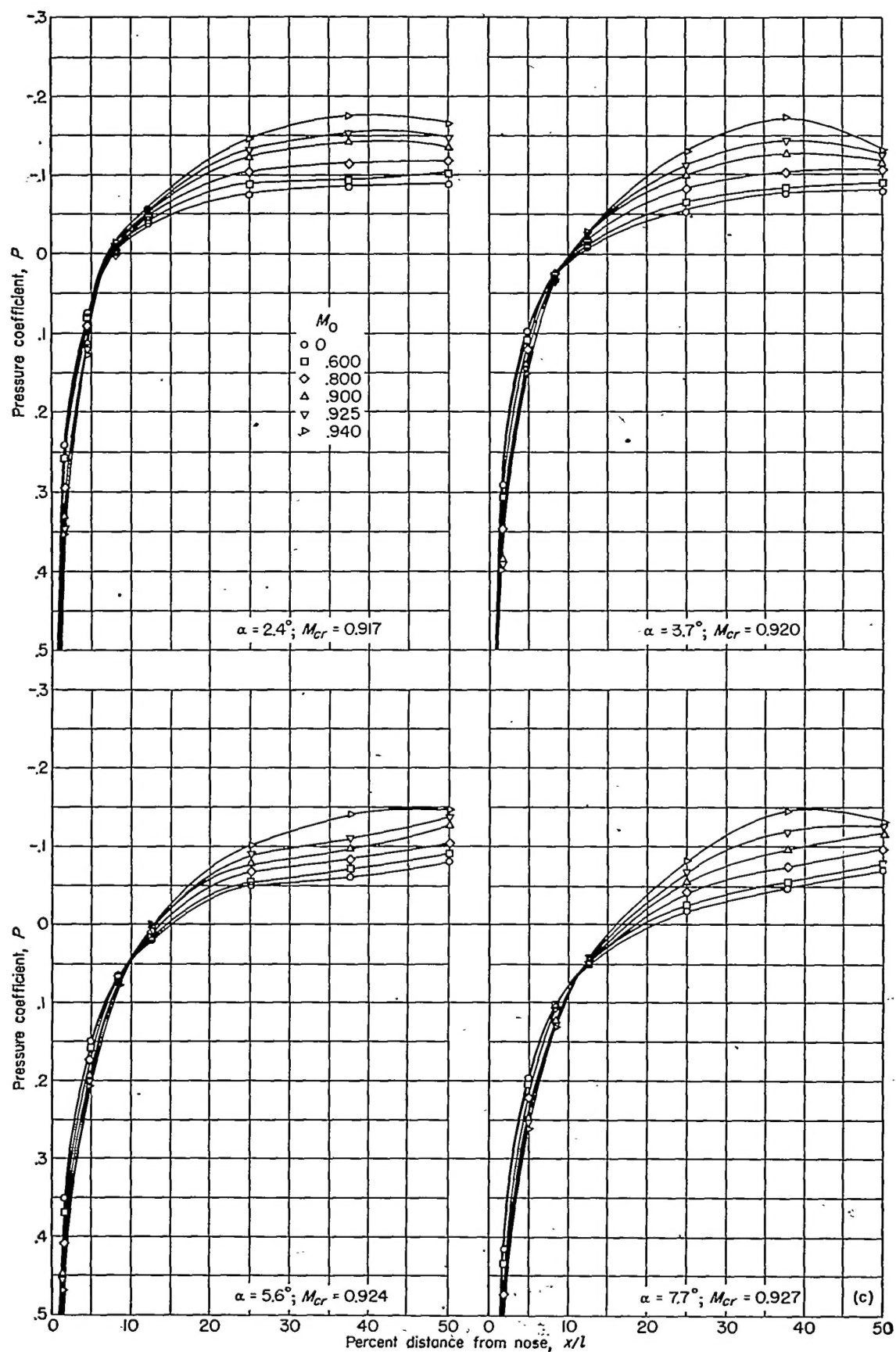
(b) $\omega = 90°$.

Figure 3.—Continued.

(c) $\omega = 180°$

FIGURE 3.—Concluded.

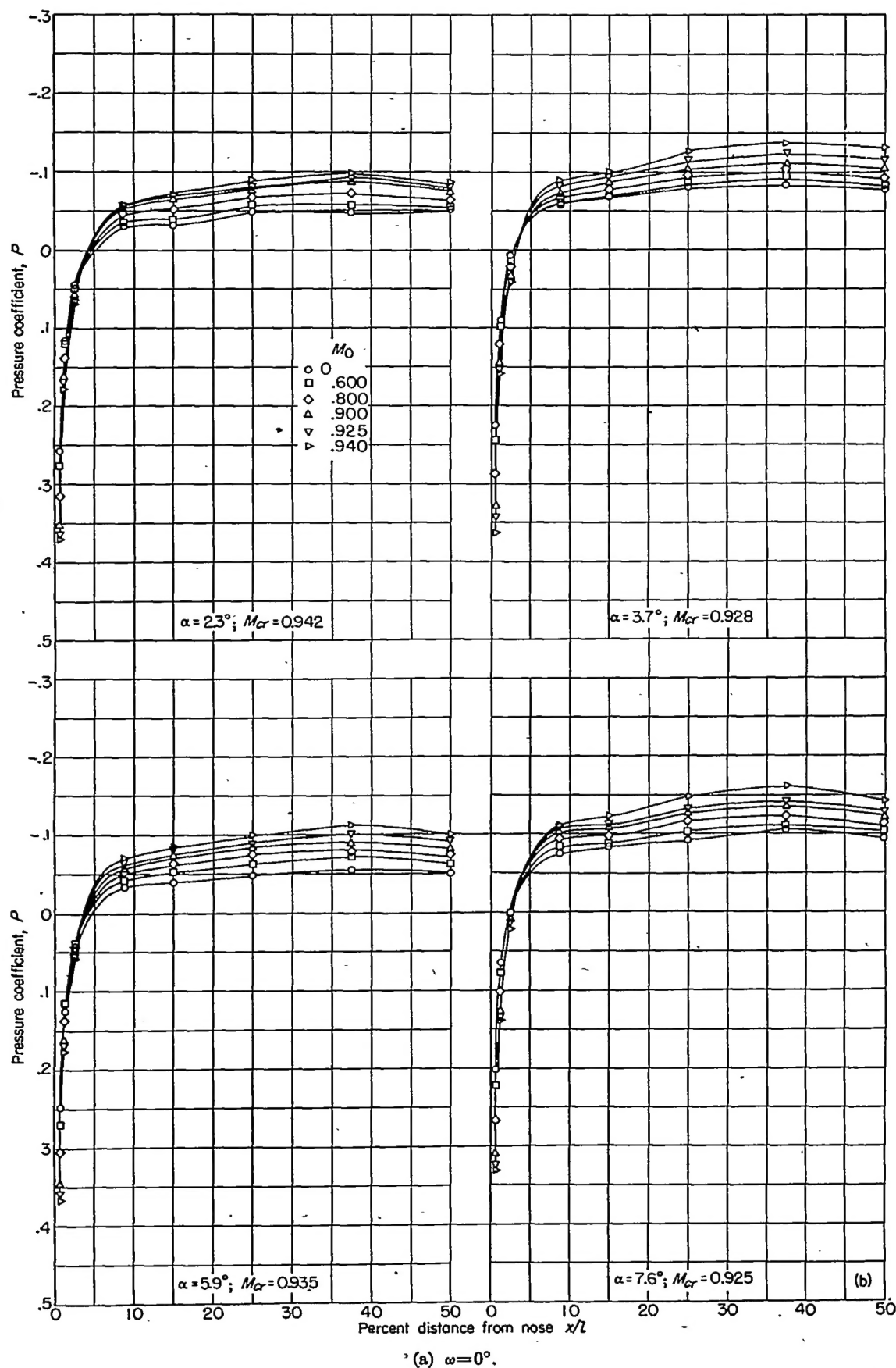(a) ω=0°.

FIGURE 4.—Experimental pressure distributions over a prolate spheroid of fineness ratio 10 at several angles of attack.
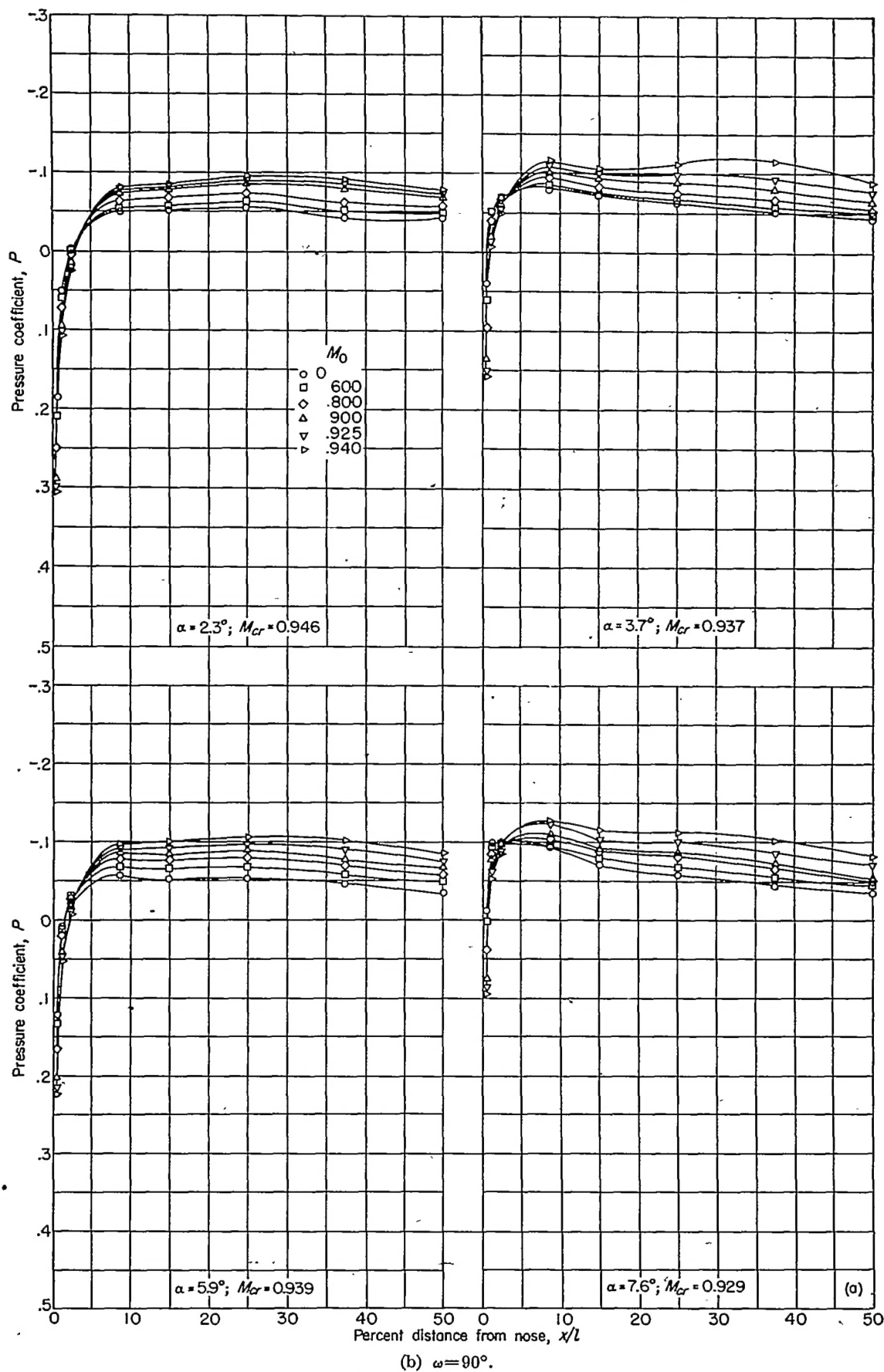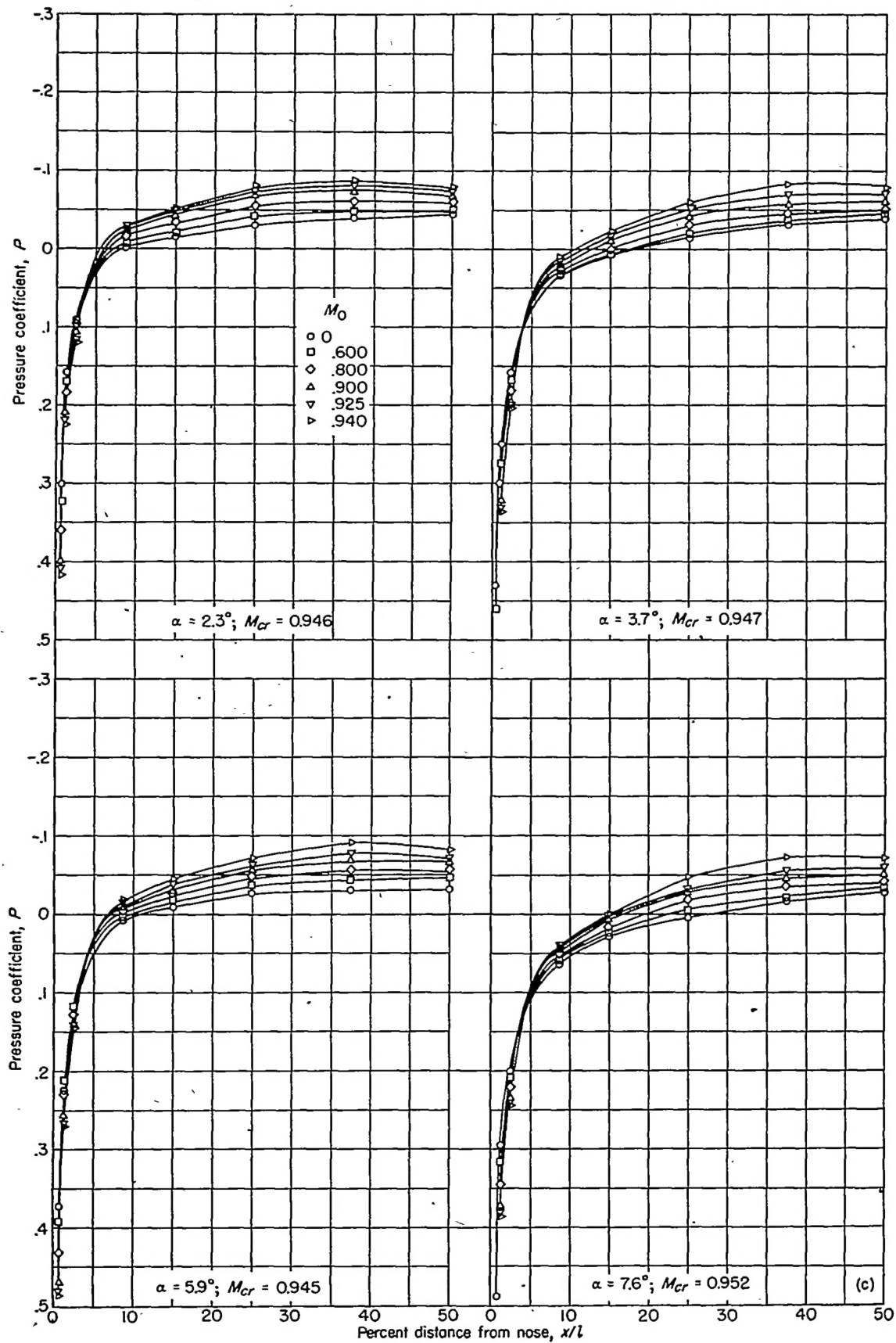
(b) $\omega = 90°$.
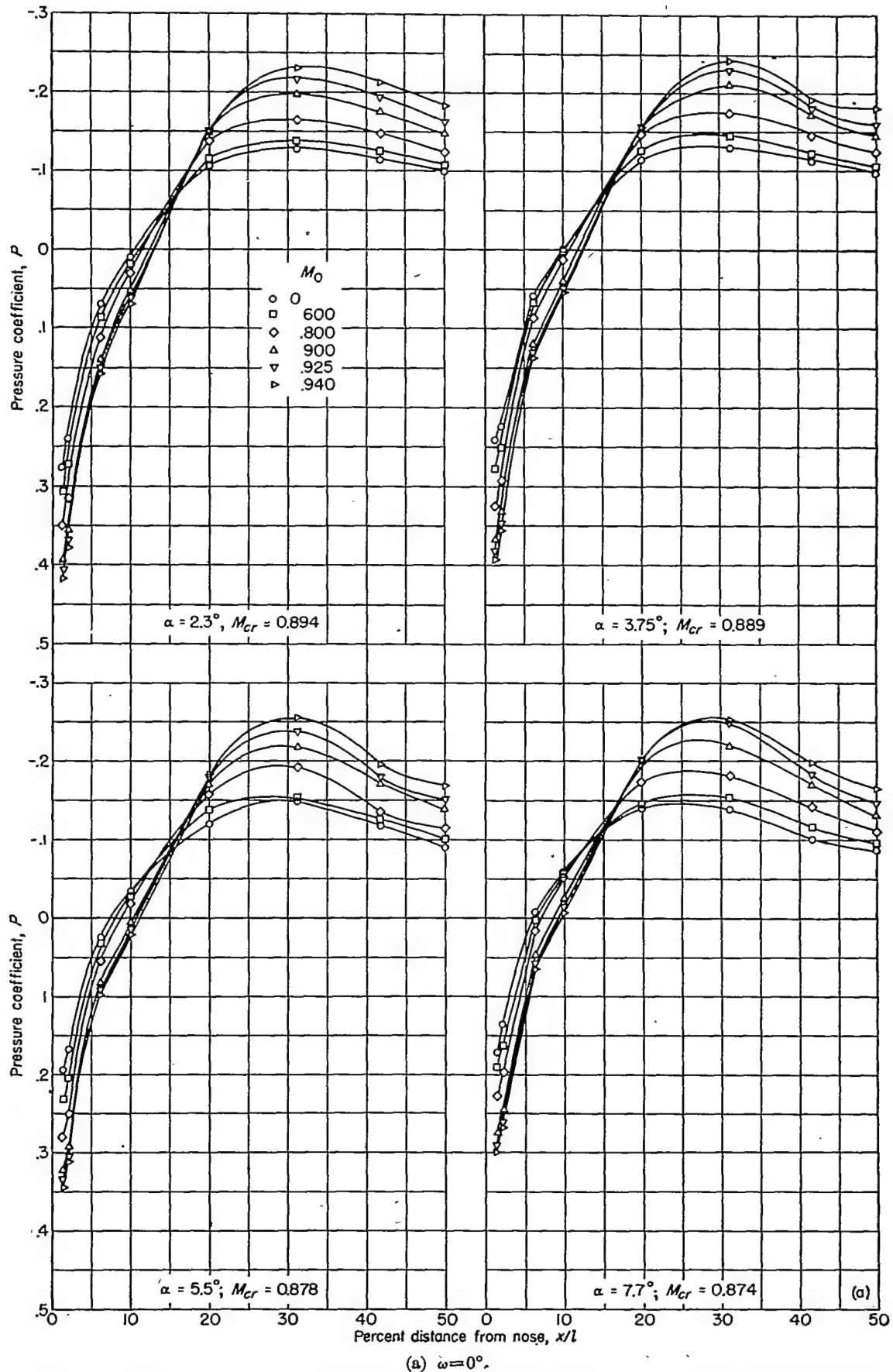
FIGURE 4.—Continued.

(c) $\omega = 180°$.

FIGURE 4.—Concluded.

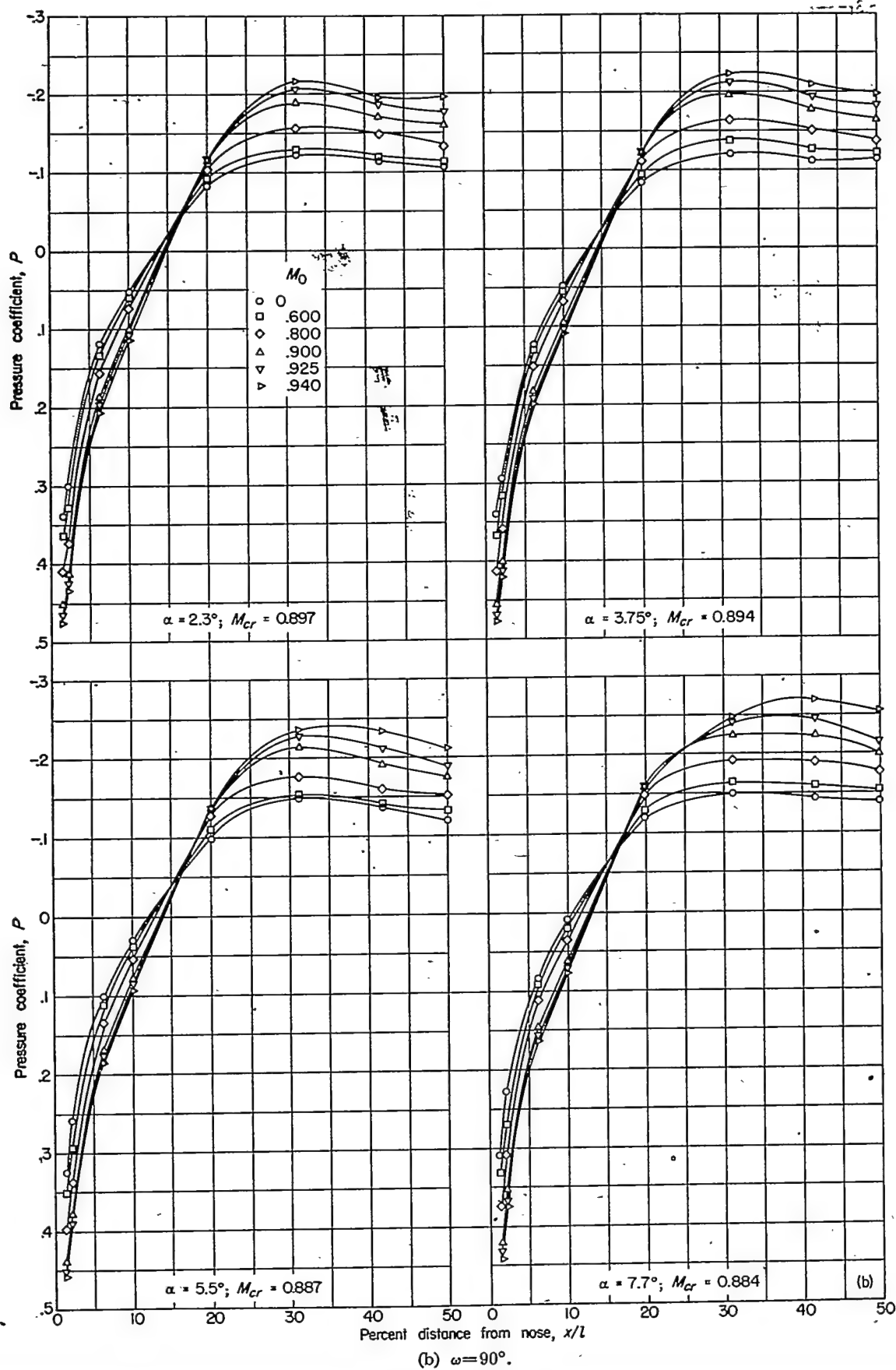FIGURE 5.—Experimental pressure distribution over a typical transonic body at several angles of attack.
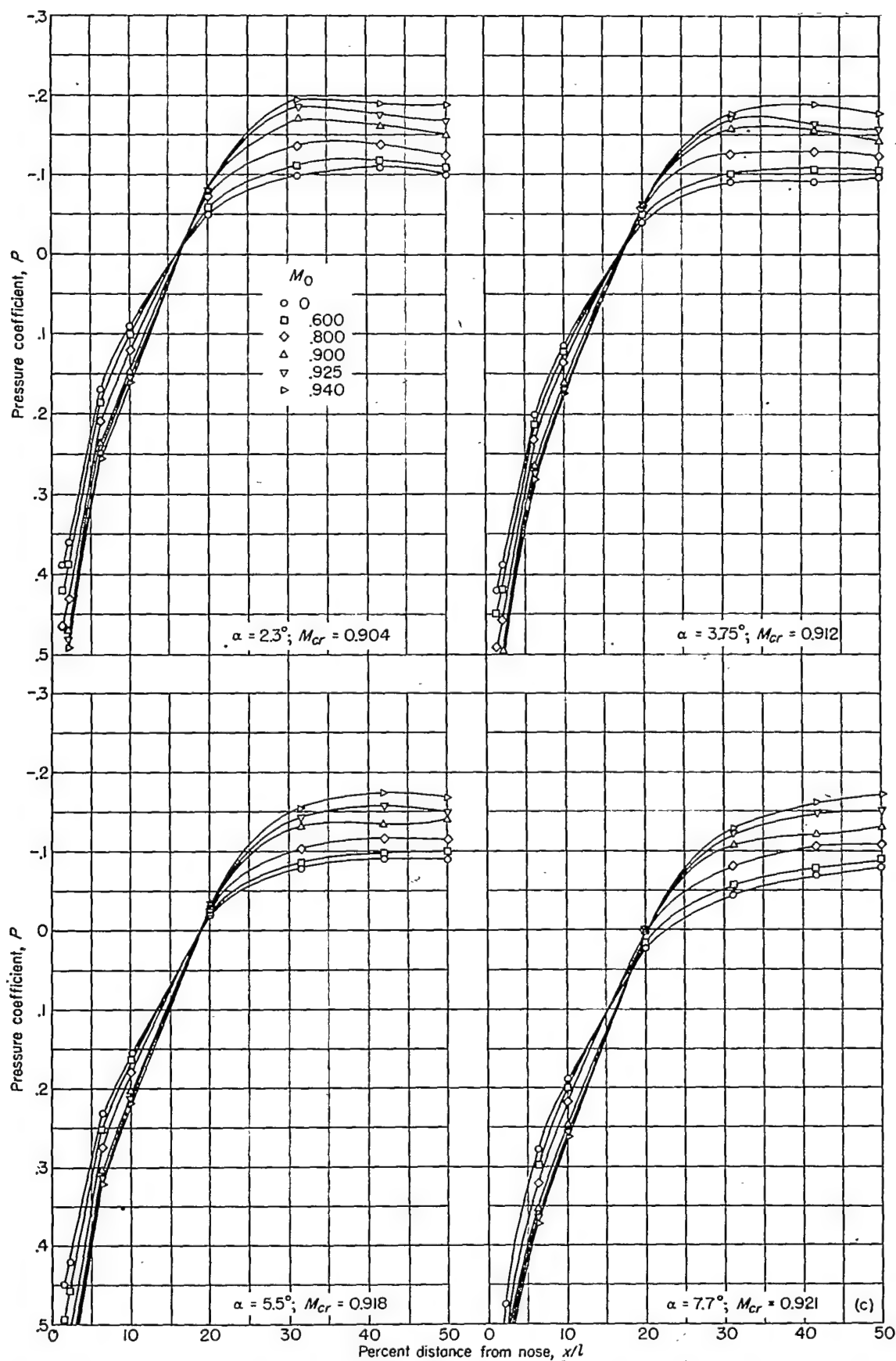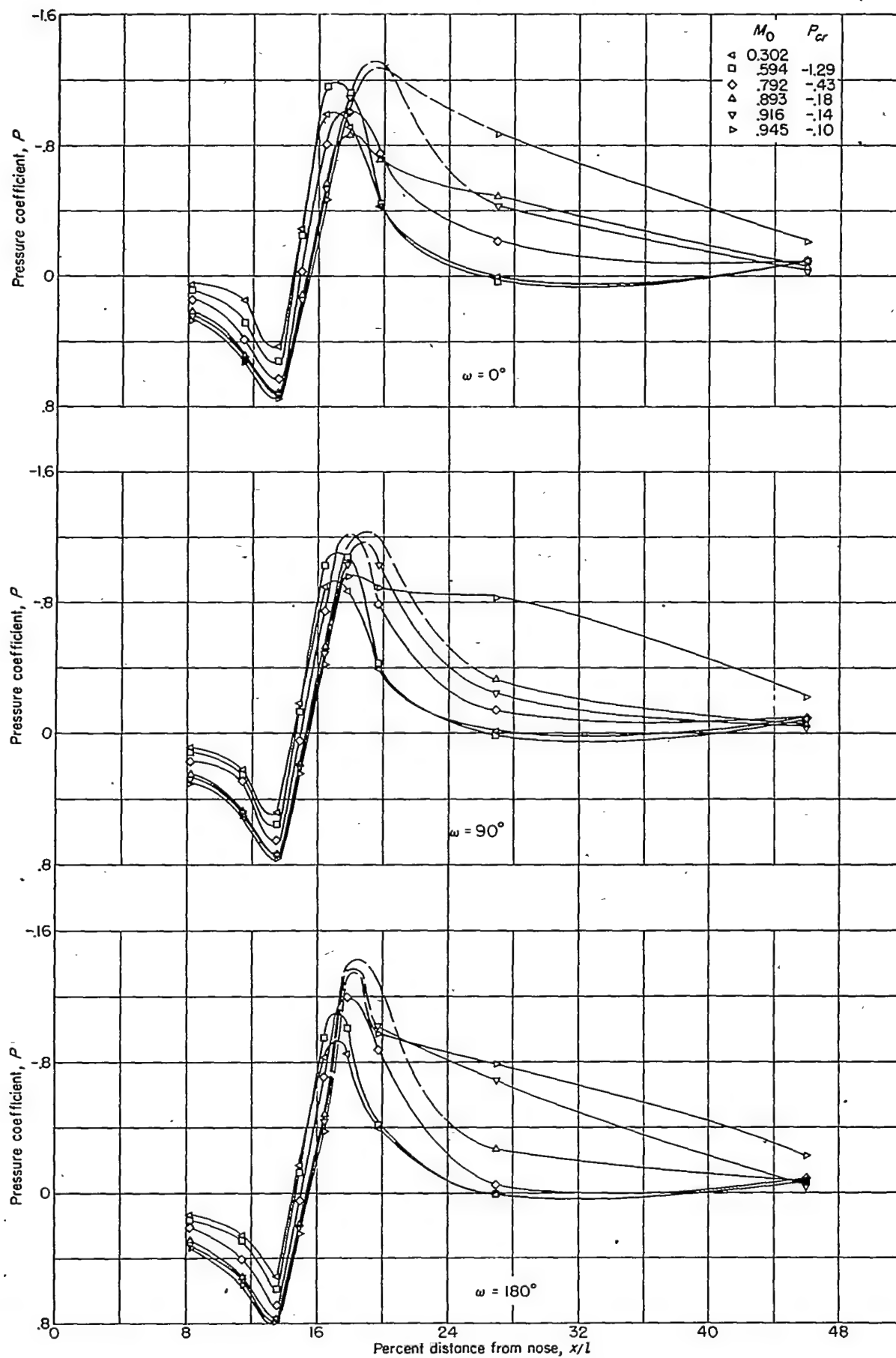
(b) $\omega = 90°$.

FIGURE 5.—Continued.

(c) $\omega=180°$.

FIGURE 5.—Concluded.

FIGURE 6.—Experimental pressure distributions over a prolate spheroid with an annular bump. $\alpha = 2.3°$.

As the flow approaches and exceeds the critical stream Mach number, a further change in the pressure distributions occurs. This change of shape (figs. 2 to 5) is essentially a rearward movement of the negative pressure peak. The nature of this change is emphasized in the plots for $M_0=0.950$ of figures 7 and 8. These figures show that the linearized theory does not predict the shift in peak pressures which occurs as the flow becomes supercritical.

The rearward shift of negative pressure peaks which occurs on the top of the body (figs. 3 (a), 4 (a), and 5 (a)) seems to be changed to a forward shift on the bottom of the body (figs. 3 (c), 4 (c), and 5 (c)). It is reasonable to assume that part or all of this forward movement of the bottom negative pressure peak may be explained by the positive pressure field which exists ahead of the under part of the sting support.

A comparison of figures 7 and 9 shows that the linearized theory gives better results for the body of larger fineness ratio. The pressures about the prolate spheroid of fineness ratio 10 are in better agreement with theory even for the stream Mach number of 0.950 than are the pressures about the body of fineness ratio 6. It may also be observed that the theoretical pressures about the prolate spheroid of fineness ratio 10, which are calculated by the two different methods, are in excellent agreement; thus, these results show that, for bodies of fineness ratios of 10 or greater, the simpler method of computing pressures presented in references 2 to 4 is fairly reliable.

INFLUENCE OF CHANGING NOSE SHAPE

The effects of changing the shape of the nose of a body are seen by comparing figures 2 (a) and 3 with figures 2 (c) and 5. The incompressible pressure distribution is changed as may be expected. However, the nature of the effect of compressibility is the same for this body as for the prolate spheroid of fineness ratio 6. The incremental pressure changes are almost the same, and the rotation and shifts of pressure peaks are very similar for both bodies. This comparison shows that the effects of compressibility do not depend to a great extent on body shape so long as the body does not depart from the specifications required for the application of the linearized equations.
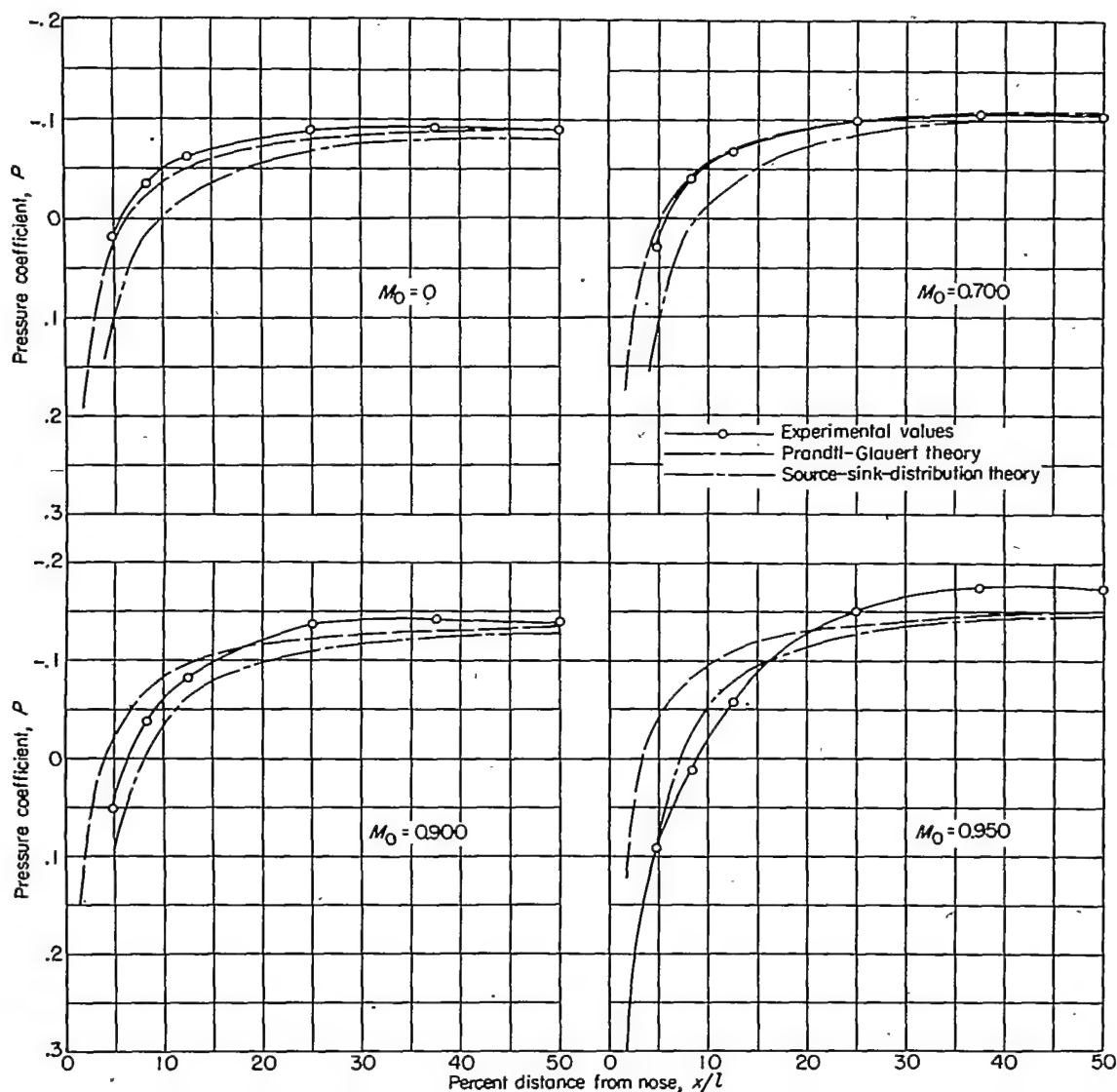

FIGURE 7.—Comparison of experimental and theoretical pressures over a prolate spheroid of fineness ratio 6 at zero angle of attack.
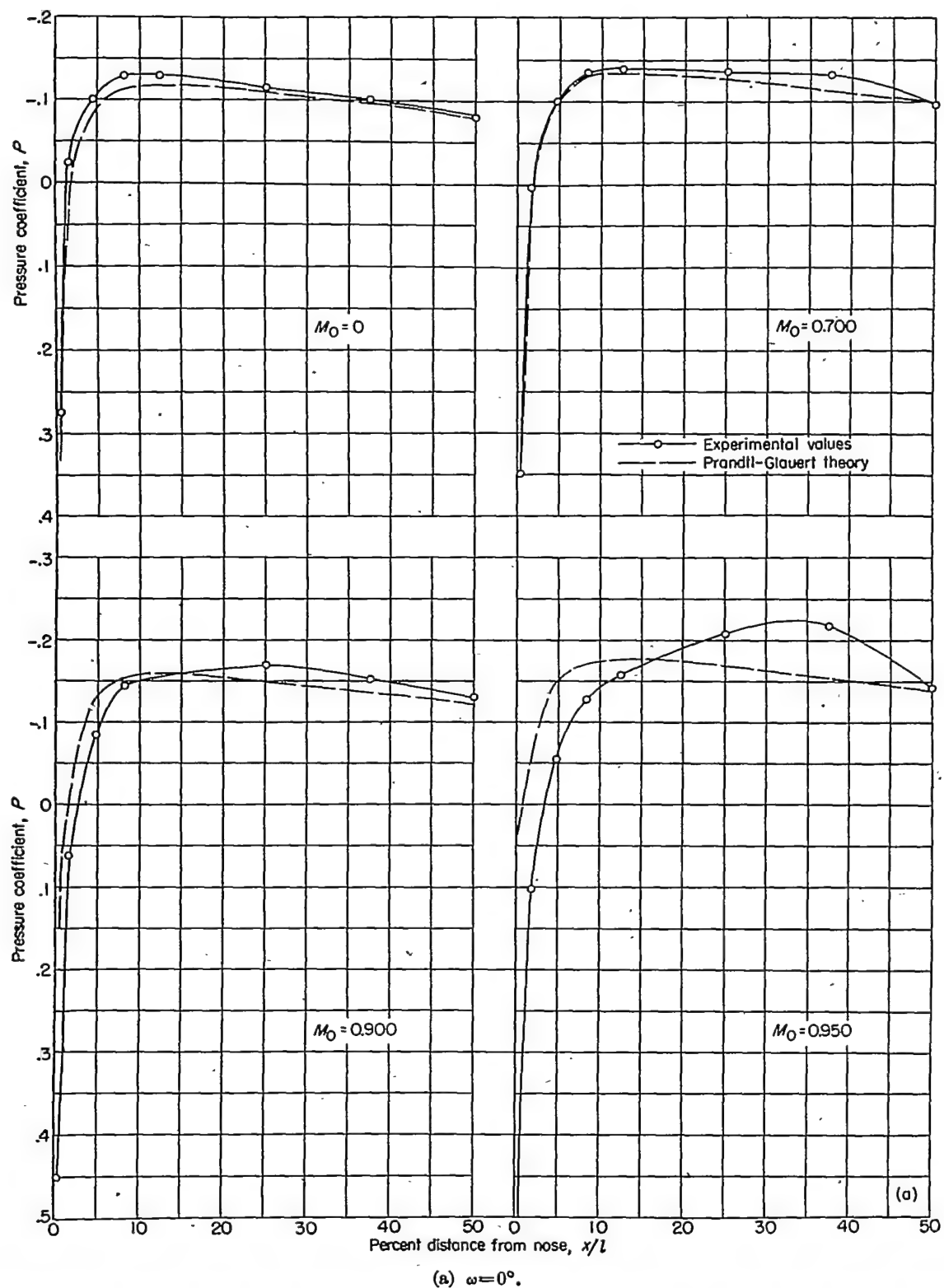
(a) $\omega=0°$.

FIGURE 8.—Comparison of experimental and theoretical pressures over a prolate spheroid of fineness ratio 6 at 5.6° angle of attack.

(b) $\omega = 90°$.
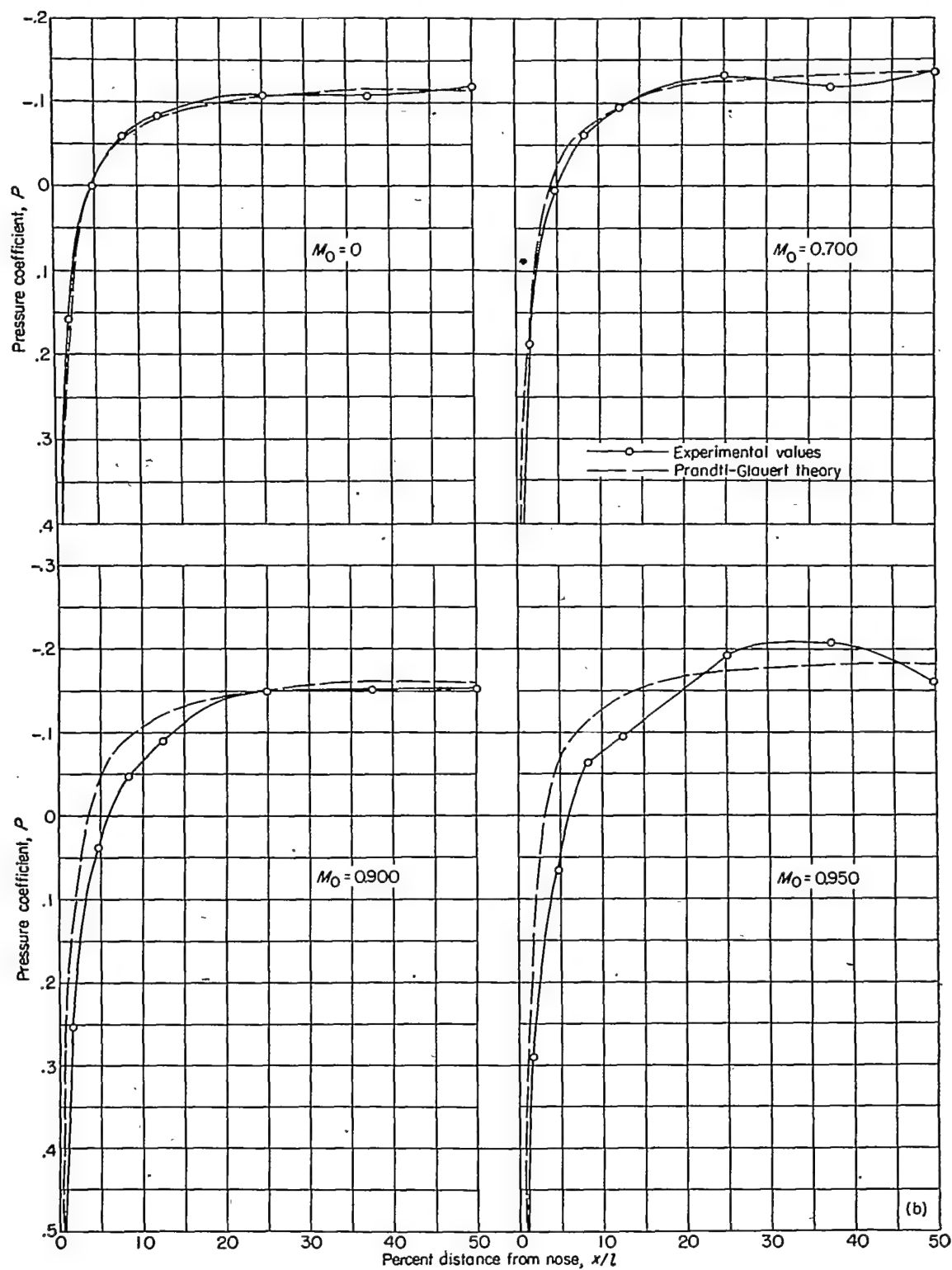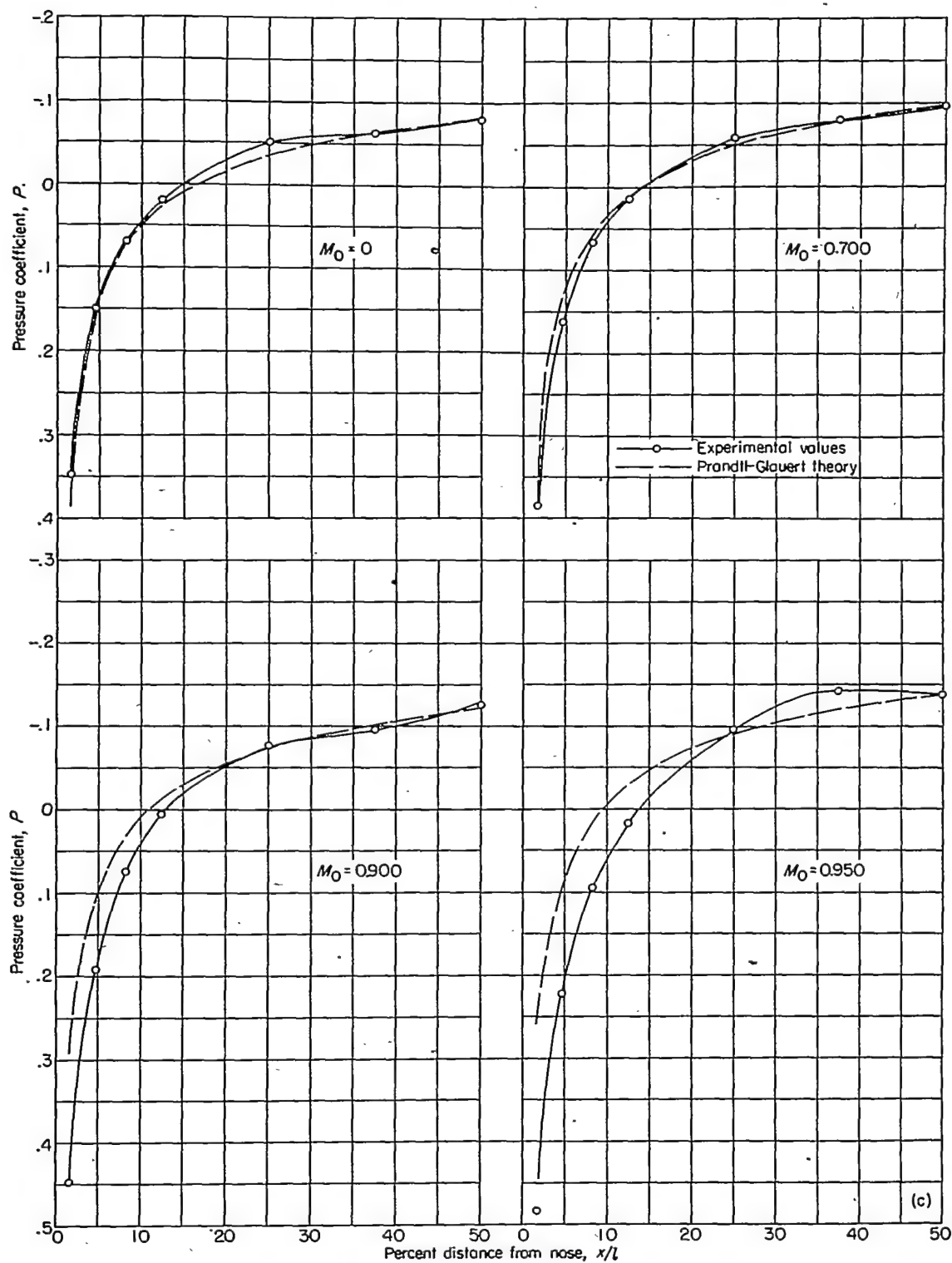
FIGURE 8.—Continued.

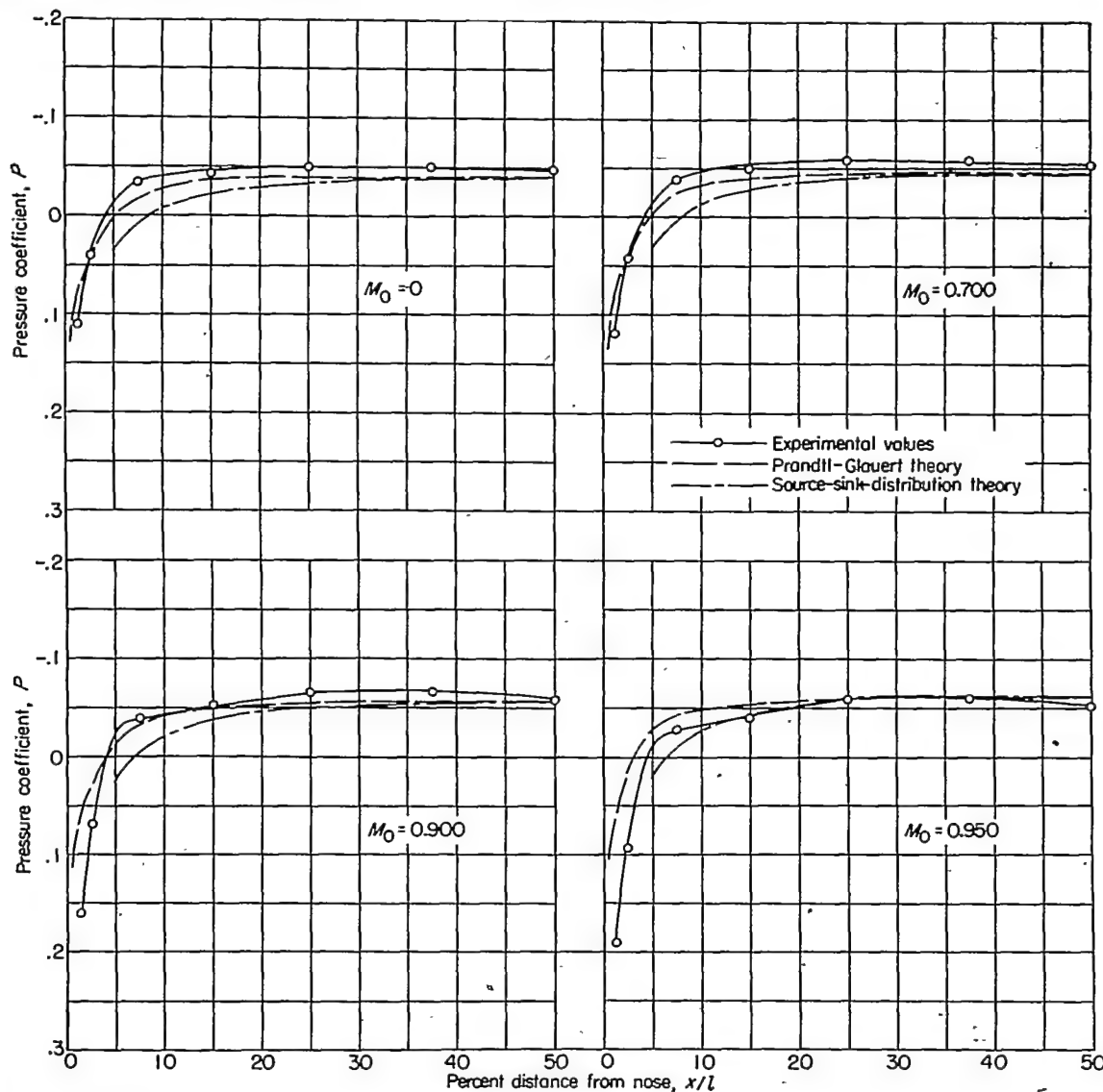(c) $\omega = 180°$;

FIGURE 8.—Concluded.

FIGURE 9.—Comparison of experimental and theoretical pressures of a prolate spheroid of fineness ratio 10 at zero angle of attack.

INFLUENCE OF FINENESS RATIO

The influence of fineness ratio on the effects of compressibility may be observed by comparing figures 2 (a) and 3 with figures 2 (b) and 4. These figures show that increasing the fineness ratio reduces the changes in pressure caused by varying the stream Mach number. This effect is predicted by the linearized theory in equation (5). It may also be observed that the pressure peaks are less prominent and do not shift their location to the extent found for the bodies of lower fineness ratio. The changes in the shape of the pressure distributions are also reduced and comparable changes occur at higher Mach numbers. The delay in the change of the shape of the pressure distribution is demonstrated by comparing figures 7 and 9 at $M_0=0.95$. For the prolate spheroid of fineness ratio 6 a marked change in the pressure distribution has already occurred, whereas for the body of fineness ratio 10 the shape of the pressure-distribution curve is almost the same as at lower Mach numbers. A consideration of the observed effects of increasing the fineness ratio indicates that such a change definitely reduces the effects of compressibility.

INFLUENCE OF ANGLE OF ATTACK

It may be shown by the use of the linearized theory that, at least to a first approximation, the lift and moment forces on a body of revolution are not affected by changes in Mach number. (See ref. 4.) The validity of this prediction is demonstrated in figure 10 which shows that the variation of the normal-force coefficient with Mach number is small for both the $f=10$ and $f=6$ prolate spheroids.
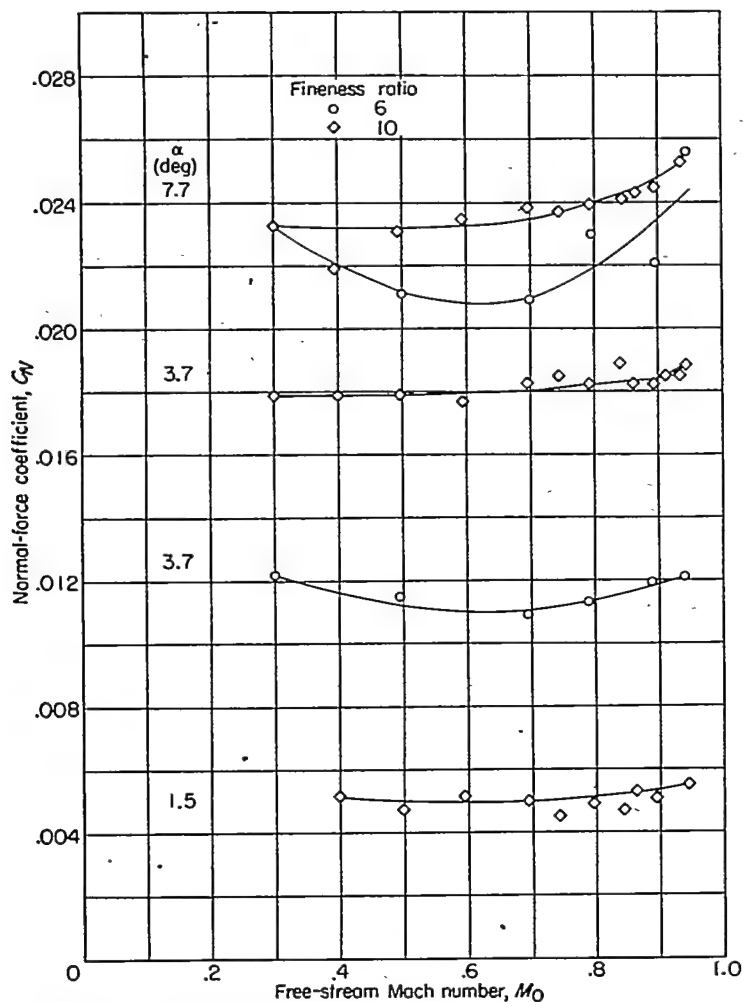
FIGURE 10.—The effect of compressibility on the normal-force coefficients over the forward half of two prolate spheroids of fineness ratios 6 and 10:

FIGURE 11.—Experimental pressure distributions over a prolate spheroid with an annular bump. $\alpha = 0°$.

INFLUENCE OF AN ANNULAR BUMP

A study of the effects of compressibility on the velocities about an infinitely long body containing surface waves (ref. 9) shows that these effects become two-dimensional in nature when the length of the surface waves becomes small with respect to the body radius. Since an annular bump on a body of revolution approximates these conditions, the flow over such a bump may also be expected to show two-dimensional effects. An examination of figures 2 (d) and 6 shows that the range of pressure coefficients found in the flow over a prolate spheroid with an annular bump is of the same order as that found in two-dimensional flow. The two-dimensional nature of the flow over an annular bump is further demonstrated by comparing the pressure coefficients with the Von Kármán relationship (ref. 10) for the effects of compressibility on two-dimensional flow (fig. 11). Figure 11 shows fair agreement between the Von Kármán relation and the experimental relationships for those regions of the body where the flow does not separate and the slope of the body is reasonably small; namely, the 8.33-, 11.5-, 13.6-, 16.5-, 17.9-, and 19.8-
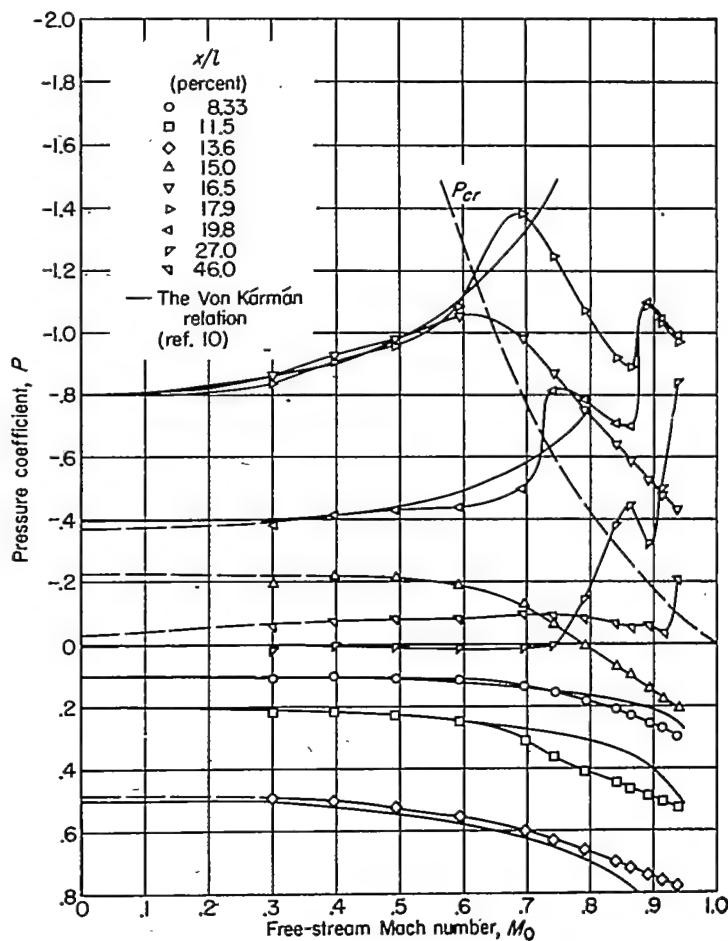
percent stations. The 15-percent station is highly irregular and cannot be explained by either two- or three-dimensional theories. The other stations are severely affected by separation phenomena. The Von Kármán relation, however, fails to explain the phenomena once the critical speed is exceeded.

CORRECTION OF INCOMPRESSIBLE PRESSURE DISTRIBUTIONS FOR THE EFFECTS OF COMPRESSIBILITY

Equations (5) and (6) suggest that an incompressible pressure distribution might be corrected for the effects of compressibility by considering a pressure-increment type of function such as $P_c - P_i$ or a rate-of-increase type of function such as P_c/P_i. In order to show whether the effects of compressibility may be expressed by such functions, a number of the pressures over the regular bodies at zero angle of attack have been plotted in figure 12 in terms of P_c/P_i and $P_c - P_i$ against x/l and M_0. Tunnel-wall corrections have been omitted, but the omission does not affect the conclusions. An examination of both functions shows that, except at supercritical Mach numbers, the values of P_c/P_i and $P_c - P_i$ are roughly constant between the 25-percent and the 50-percent stations. Over the forward part of the body, the values are more variable.
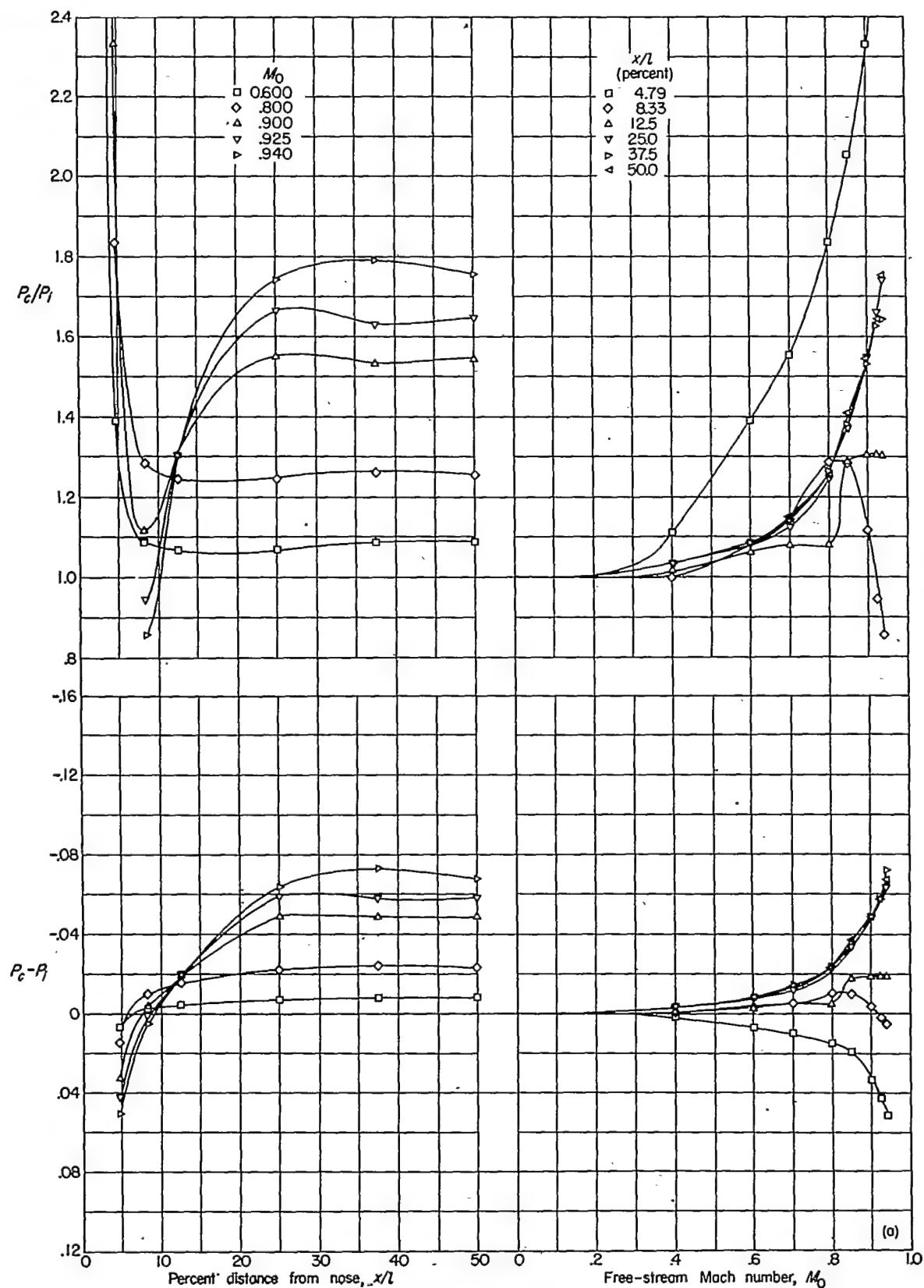
(a) Prolate spheroid; $f=6$.

FIGURE 12.—Experimental compressibility correction functions as determined by the flow over three regular bodies of revolution at zero angle of attack.
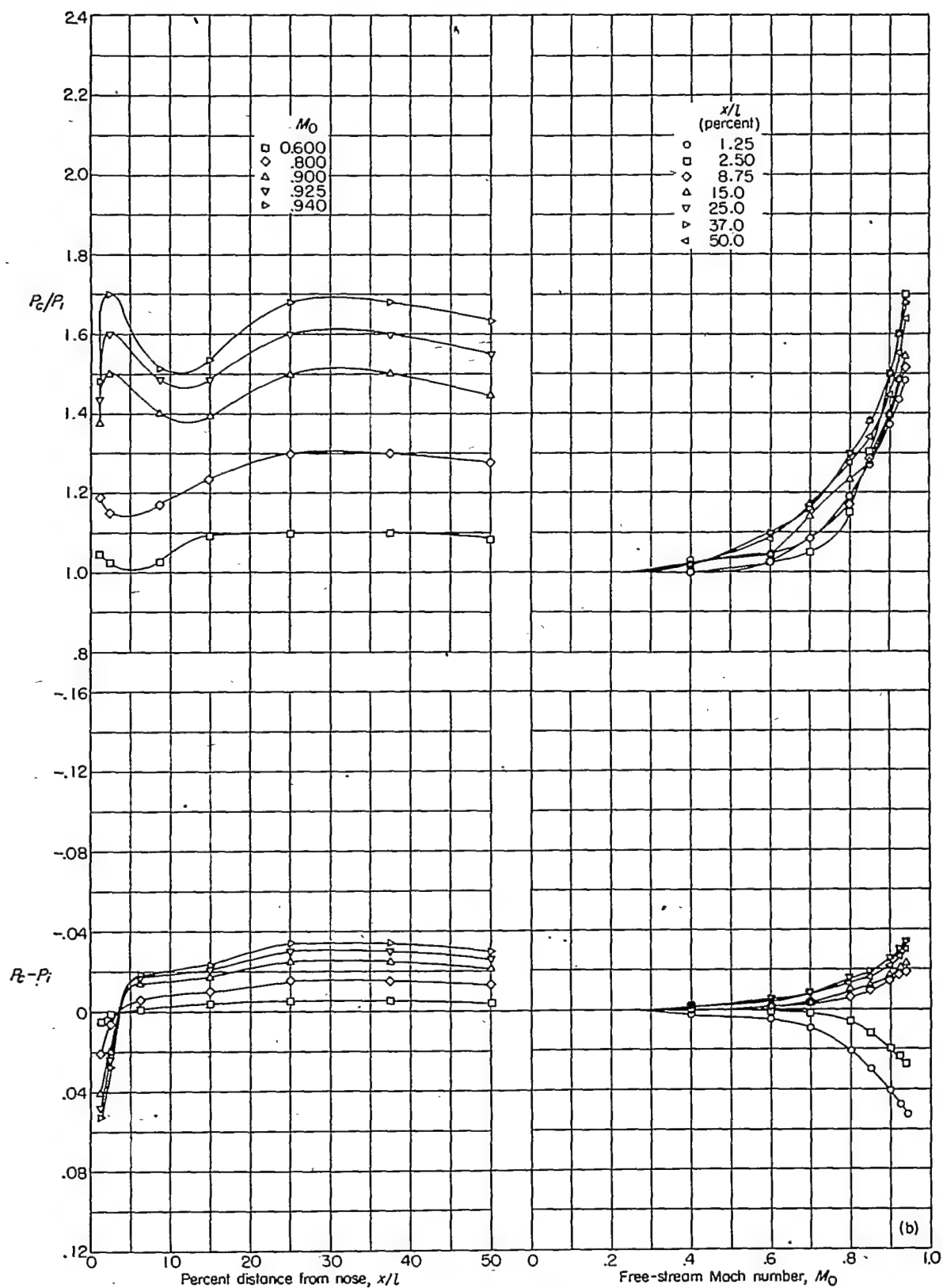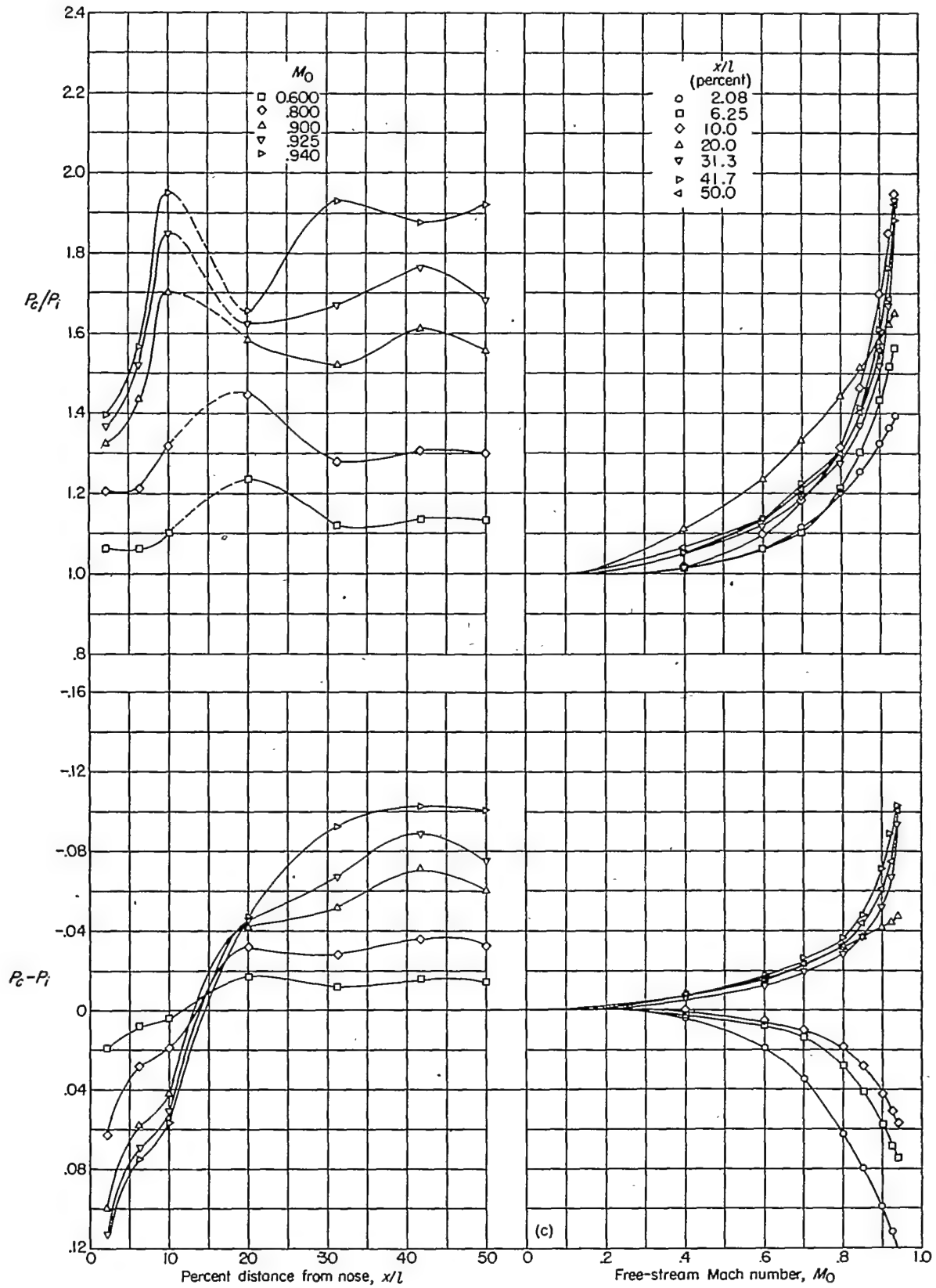
(b) Prolate spheroid; $f=10$.

FIGURE 12.—Continued.

(c) Typical transonic body.

FIGURE 12.—Concluded.

The P_c/P_i function becomes discontinuous in the neighborhood of $P_i=0$. This behavior may be attributed to the fact that the pressure coefficient is zero at the incompressible stream-pressure point and, since one of the effects of compressibility is to shift the stream-pressure point, discontinuities may be expected in the neighborhood of this point. However, since the pressures in this region are small, a wide variation in P_c/P_i may be permissible without serious error in the corrected results.

The P_c-P_i correction may also be expected to become irregular in the region of the nose. The experimental curves show that this function changes sign in the neighborhood of the stream-pressure point so that any correction function of this type should include the position on the body. However, such a function cannot be obtained from the linearized method as this method does not indicate the change of sign shown in the experimental data.

The experimental values of P_c-P_i and P_c/P_i at the centers of the regular bodies are compared with equations (5) and (6) in figure 13 in order to show the validity of the prediction of the effect of compressibility by the linearized potential-flow theory. It is observed that equation (6)
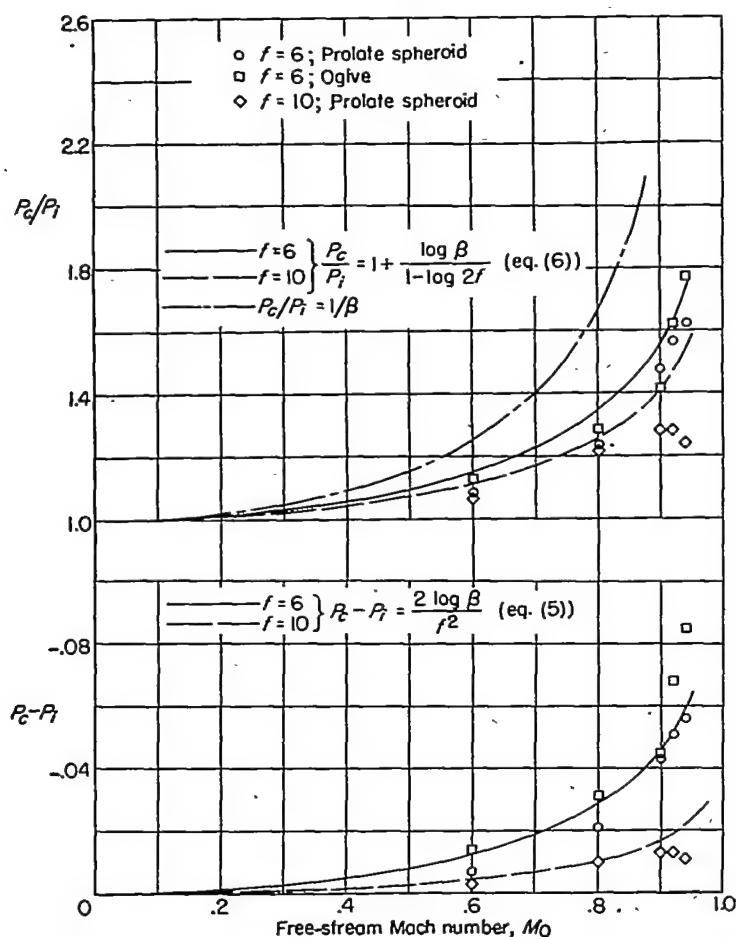
within its limitations predicts the effects of compressibility for three-dimensional flow whereas the relation $\frac{P_c}{P_i}=\frac{1}{\beta}$, which is used to predict the compressibility effects of two-dimensional flow, does not. It may also be observed that equations (5) and (6) predict the effects of compressibility with about the same degree of accuracy.

The correction functions are applied to several incompressible pressure-coefficient distributions in figure 14, which are compared with the corresponding experimental distributions. It is shown in figure 14 (a) that increasing the fineness ratio of the prolate spheroid from 6 to 10 or reducing the bluntness of the nose, which is the essential difference between the ogival body and the prolate spheroid, extends the region of the body for which corrections can be made from the 20-percent station for the prolate spheroid of fineness ratio 6 forward at least to the 10-percent station for the sharper-nose bodies. The P_c/P_i function expresses the effect of compressibility more accurately in the vicinity of the nose than does the P_c-P_i function. This result is to be expected since one of the effects of compressibility already noted is the rotation of the pressure distribution, which is accounted for by the P_c/P_i expression but not by the P_c-P_i expression.

The increasing error which results from increasing the stream Mach number is shown in figure 14 (b). At $M_0=0.800$, the incompressible pressure coefficients about the fineness ratio 6 prolate spheroid may be corrected with a fair degree of accuracy as far forward as the 5-percent station. As the Mach number increases, the divergence between the corrected values and the experimental values in the region of the nose increases and, with still greater Mach numbers, tends to spread toward the center. At $M_0=0.940$, which is supercritical for the prolate spheroid of fineness ratio 6, the correction formulas are still applicable at the center, so that successful extrapolation of the linearized theory into the supercritical range is found to depend on the section of the body to which the extrapolation is applied.

As may be expected, the success of the linearized theory in expressing the effects of compressibility decreases as the angle of attack increases. The principal reason for this result is that an angle of attack involves a pressure peak on the forepart of the top of the body, which moves rearward when the stream Mach number approaches and exceeds the critical value for the body. Since the correction formulas either rotate or translate the incompressible pressure distribution, they cannot express this change in the shape of the pressure distribution. This phenomenon is demonstrated in figure 14 (c), which presents a comparison of the corrected pressure-coefficient distributions and the experimental distributions of the flow about the prolate spheroid of fineness ratio 6 at several angles of attack. Even though the shift of the peak pressure is not accounted for in the correction formula, the corrected distributions are not seriously in error at the peaks and the agreement improves over the midportion of the body. Thus, if some error is permissible, these formulas may be applied for angles of attack as high as 7° or 8°.

FIGURE 13.—Theoretical compressibility correction functions compared with experimental results. $\alpha=0°$; $\frac{x}{l}=50$ percent.
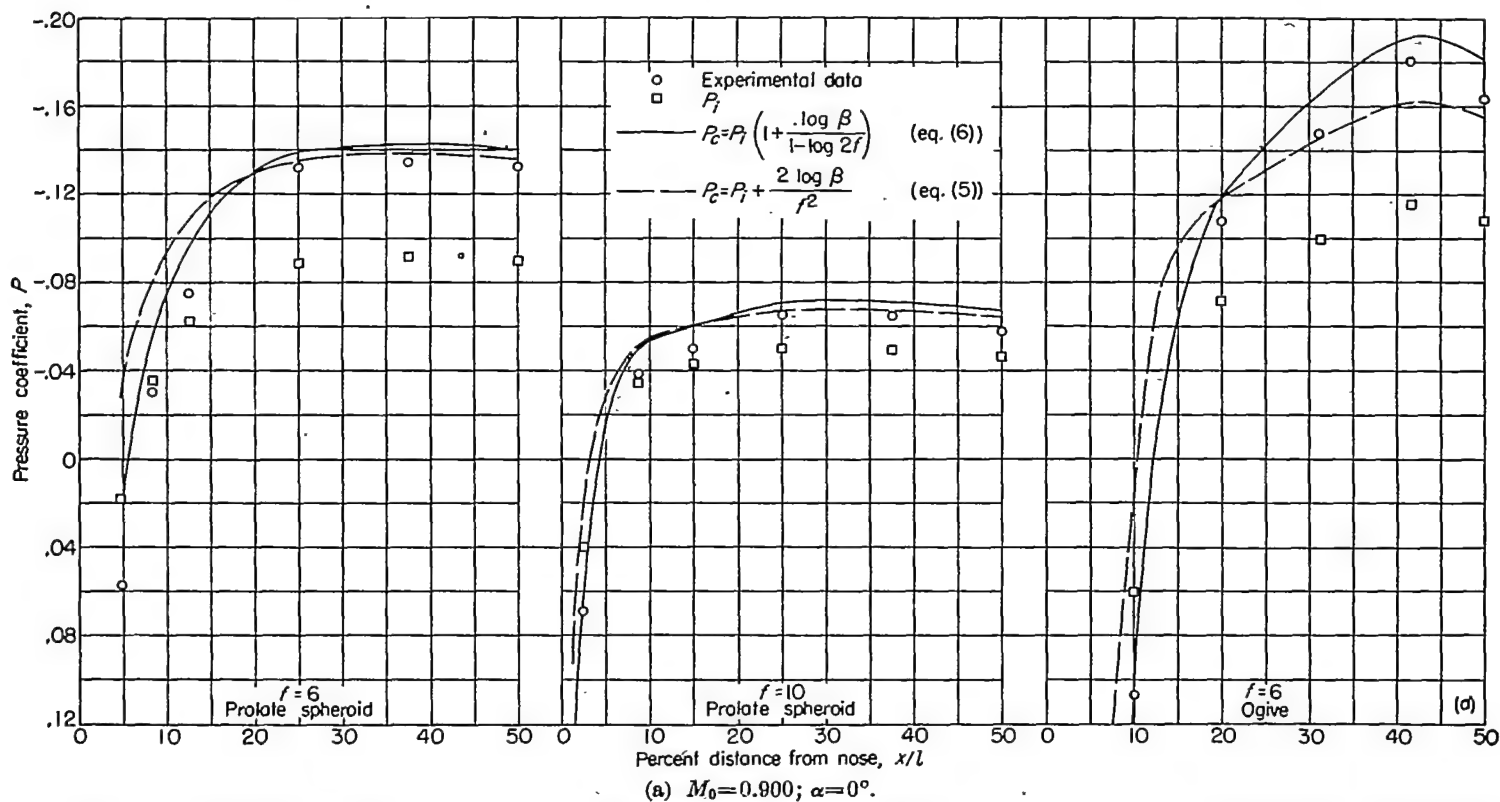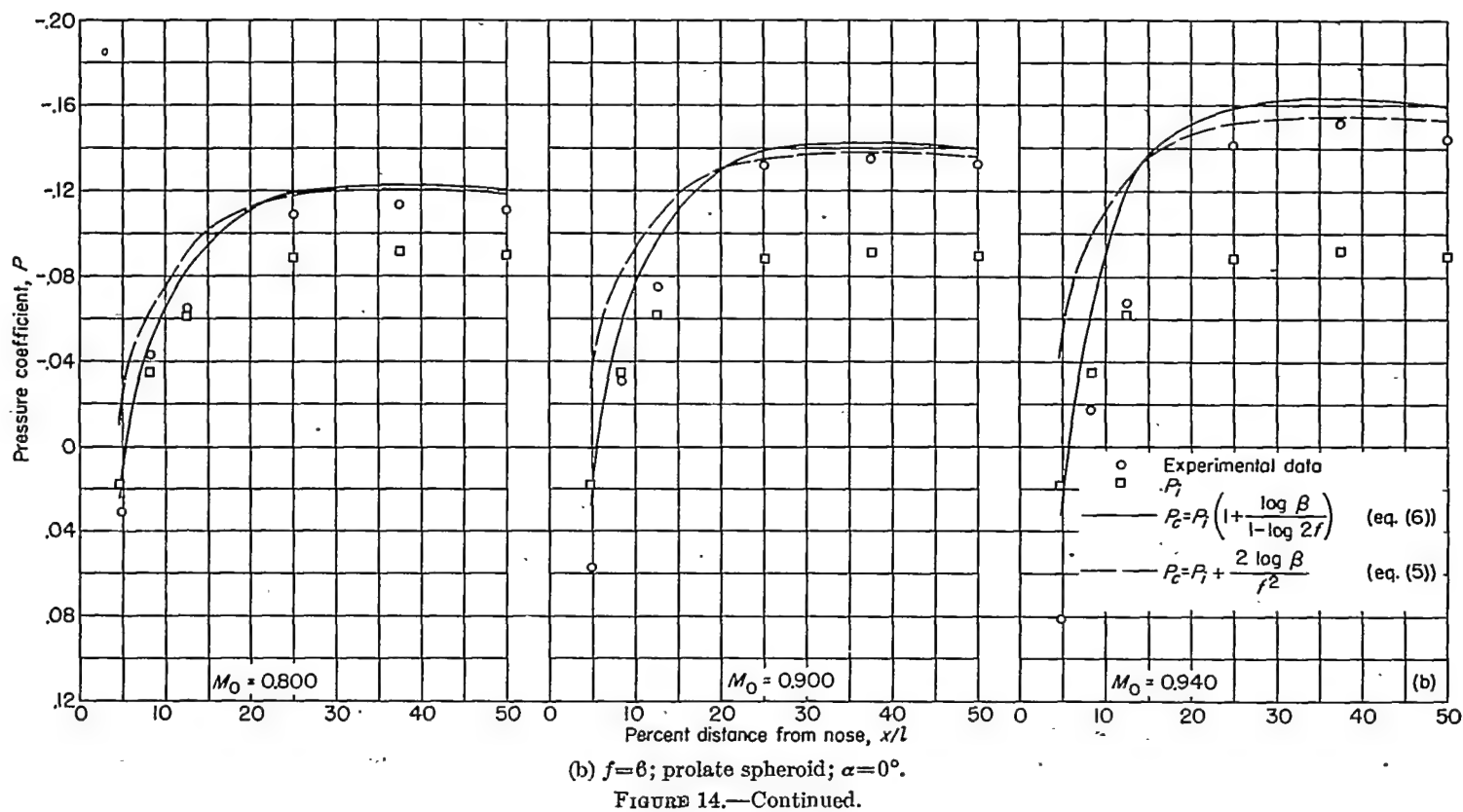
(a) $M_0 = 0.900$; $\alpha = 0°$.

FIGURE 14.—Comparison of theoretically corrected incompressible pressure-coefficient distributions with the corresponding experimental distributions.

(b) $f=6$; prolate spheroid; $\alpha = 0°$.

FIGURE 14.—Continued.

(c) $f=6$; prolate spheroid; $M_0=0.900$.
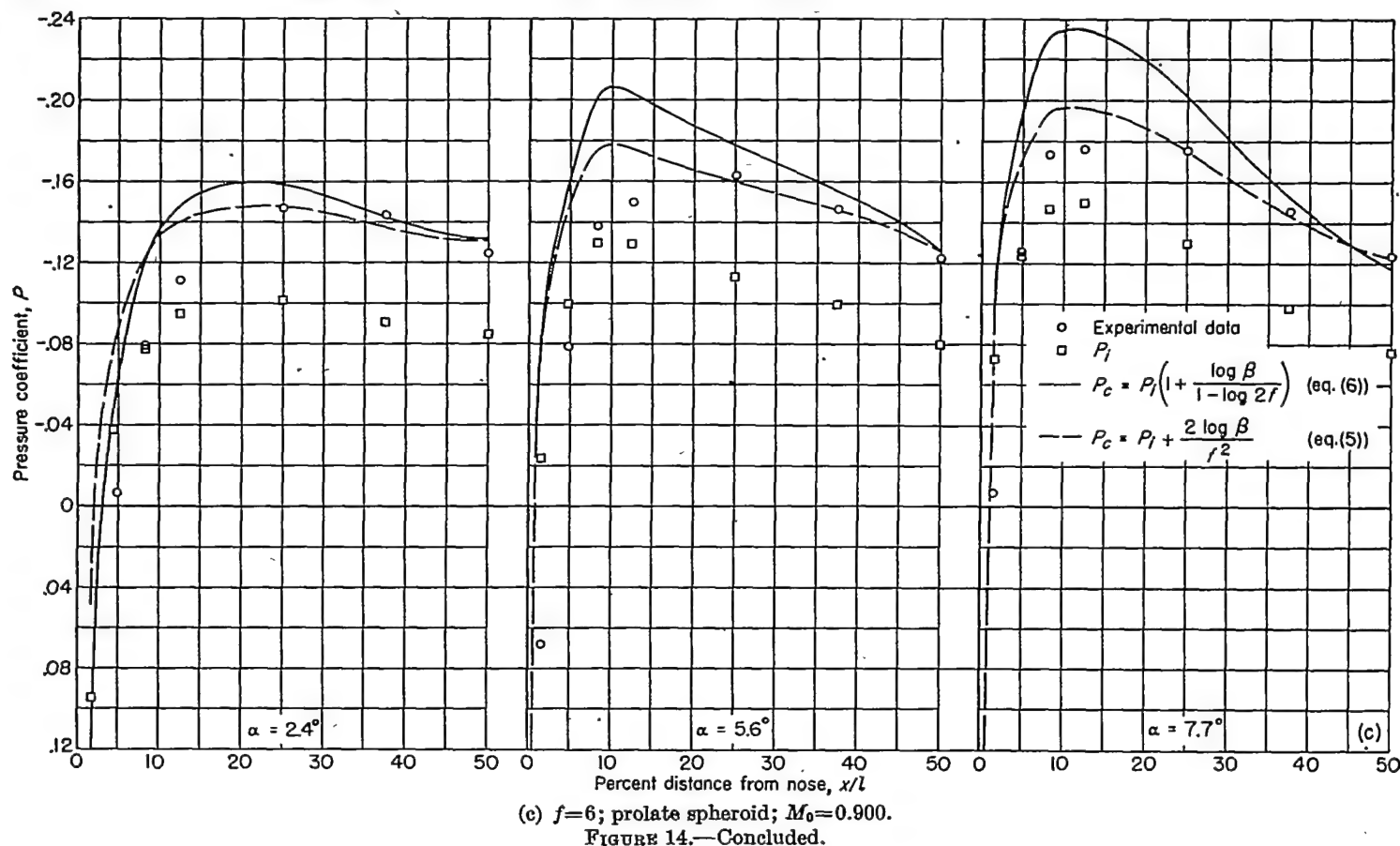
FIGURE 14.—Concluded.

Figure 14 (c) indicates that equation (6) does not correct as satisfactorily over the central parts of the body at angles of attack as equation (5). This lack of agreement is due to the compressibility effect on the lift forces. It has already been shown that the lift forces are not much affected by compressibility; hence, the increments of the pressure coefficients due to compressibility are about the same for the top and bottom of the body. Since the absolute values of the pressure coefficients are less on the bottom of the body and greater on the top than if the lift forces had not been present, equation (6) will overcorrect the pressure coefficients on the top and undercorrect those on the bottom. The same reasoning shows that equation (5), which gives a constant increment over the entire body, will express the compressibility effect with an angle of attack better over the central part of the body to which it applies than will equation (6).

CONCLUSIONS

The results of the tests made on several bodies of revolution have shown the following effects of compressibility on three-dimensional flow:

1. In general, the compressibility effect is to increase the pressure differences over a body of revolution. The pressure distributions are approximately rotated about a point near stream-pressure and the negative-pressure peaks are moved rearward.

2. The linearized modification of the compressible potential-flow equation will predict the pressures over the central part of the body but will not predict the changes in pressure ahead of the stream-pressure point nor will it predict the change in shape which occurs with supercritical flow.

3. The correction formulas

$$\frac{P_c}{P_i}=1+\frac{\log\beta}{1-\log 2f}$$

and

$$P_c-P_i=\frac{2\log\beta}{f^2}$$

(where P_c and P_i are the pressure coefficients for compressible and incompressible flow, respectively, f is the fineness ratio, and $\beta=\sqrt{1-M_0^2}$ in which M_0 is the Mach number) may be used approximately to correct incompressible-flow pressures over the central part of streamline thin bodies of revolution; the errors will increase as the supercritical Mach number is approached and exceeded. Since P_c/P_i rotates the pressure distribution, this correction is better to use at zero angle of attack; however, the form P_c-P_i expresses the effects of angle of attack more correctly and should be used when an angle of attack other than zero is involved.

4. The effects of compressibility are approximately the same for various bodies of the same fineness ratio, provided the body shape satisfies the requirements of the linearized theory.

5. Increasing the fineness ratio tends to reduce the effects of compressibility.

6. The effects of compressibility on an annular protuberance of short chord on a body of revolution tend to follow more nearly two-dimensional laws than three-dimensional laws.

7. Lift forces and moments over the forward part of the body are relatively unaffected by compressibility.

LANGLEY AERONAUTICAL LABORATORY,
     NATIONAL ADVISORY COMMITTEE FOR AERONAUTICS,
       LANGLEY FIELD, VA., *November 5, 1951.*

APPENDIX A

DERIVATION OF THE EQUATIONS FOR THE COMPRESSIBLE PRESSURE COEFFICIENTS OF THE FLOW ABOUT A PROLATE SPHEROID

The solution of the linearized compressible-flow equation for a prolate spheroid requires a derivation of the relation for the incompressible velocities about the body. The incompressible velocities about a prolate spheroid are defined by the potential equations given in reference 5. These equations may be combined and written

$$\varphi = U\mu\zeta\cos\alpha + A(\cos\alpha)\mu\left(\frac{1}{2}\zeta\log\frac{\zeta+1}{\zeta-1}-1\right)+$$

$$B(\sin\alpha)\sqrt{1-\mu^2}\sqrt{\zeta^2-1}\left(\frac{1}{2}\log\frac{\zeta+1}{\zeta-1}-\frac{\zeta}{\zeta^2-1}\right)\cos\omega \quad (7)$$

The values of the constants A and B which satisfy the required boundary conditions are

$$A=\frac{U}{\dfrac{\zeta_0}{\zeta_0{}^2-1}-\dfrac{1}{2}\log\dfrac{\zeta_0+1}{\zeta_0-1}}$$

$$B=\frac{U}{\dfrac{\zeta_0{}^2-2}{\zeta_0(\zeta_0{}^2-1)}-\dfrac{1}{2}\log\dfrac{\zeta_0+1}{\zeta_0-1}}$$

where ζ_0 is the value of the coordinate which represents the body. It may be shown that the eccentricity of the ellipse $e=\sqrt{\dfrac{l^2-4b^2}{l^2}}=\dfrac{1}{\zeta_0}$ where l and $2b$ are the lengths of the major and minor axes of the prolate spheroid. Since the fineness ratio f is equal to $l/2b$, $e=\sqrt{1-\dfrac{1}{f^2}}$. The incompressible velocities are transformed to the u, v, and w components by the following equations:

velocity components obtained by differentiating the potential equation are

$$\left.\begin{aligned}
\frac{u^*}{U}&=\frac{1-\mu^2}{1-e^2\mu^2}K_a\cos\alpha-\frac{\mu\sqrt{(1-\mu^2)(1-e^2)}}{1-e^2\mu^2}K_b\cos\omega\sin\alpha\\[2mm]
\frac{v^*}{U}&=-\frac{\mu\sqrt{(1-\mu^2)(1-e^2)}}{1-e^2\mu^2}K_a\cos\omega\cos\alpha\\[2mm]
&\quad+\frac{\mu^2(1-e^2)}{1-e^2\mu^2}K_b\cos^2\omega\sin\alpha+K_b\sin^2\omega\sin\alpha\\[2mm]
\frac{w^*}{U}&=-\frac{\mu\sqrt{(1-\mu^2)(1-e^2)}}{1-e^2\mu^2}K_a\sin\omega\cos\alpha\\[2mm]
&\quad+\frac{\mu^2(1-e^2)}{1-e^2\mu^2}K_b\sin\omega\cos\omega\sin\alpha-K_b\sin\omega\cos\omega\sin\alpha
\end{aligned}\right\} \quad (8)$$

where

$$\left.\begin{aligned}
K_a&=1-\frac{\log\left(\dfrac{1+e}{1-e}\right)-2e}{\log\left(\dfrac{1+e}{1-e}\right)-\dfrac{2e}{1-e^2}}\\[3mm]
K_b&=1-\frac{\log\left(\dfrac{1+e}{1-e}\right)-\dfrac{2e}{1-e^2}}{\log\left(\dfrac{1+e}{1-e}\right)-\dfrac{2e(1-2e^2)}{1-e^2}}
\end{aligned}\right\} \quad (9)$$

and u^*, v^*, and w^* are the velocity components in a coordinate system alined with the x-axis of the body. These

$$\left.\begin{aligned}
\frac{u}{U}&=\frac{u^*}{U}\cos\alpha+\frac{v^*}{U}\sin\alpha\\[2mm]
\frac{v}{U}&=-\frac{u^*}{U}\sin\alpha+\frac{v^*}{U}\cos\alpha\\[2mm]
\frac{w}{U}&=\frac{w^*}{U}
\end{aligned}\right\} \quad (10)$$

With the preceding transformation, the velocity equations (8) become

$$\left.\begin{aligned}
\frac{u}{U}&=\frac{1}{1-e^2\mu^2}(\sqrt{1-\mu^2}\cos\alpha-\mu\sqrt{1-e^2}\cos\omega\sin\alpha)(\sqrt{1-\mu^2}K_a\cos\alpha-\mu\sqrt{1-e^2}K_b\cos\omega\sin\alpha)+K_b\sin^2\omega\sin^2\alpha\\[2mm]
\frac{v}{U}&=-\frac{1}{1-e^2\mu^2}(\sqrt{1-\mu^2}\sin\alpha+\mu\sqrt{1-e^2}\cos\omega\cos\alpha)(\sqrt{1-\mu^2}K_a\cos\alpha-\mu\sqrt{1-e^2}K_b\cos\omega\sin\alpha)+K_b\sin^2\omega\cos\alpha\sin\alpha\\[2mm]
\frac{w}{U}&=-\frac{\mu\sqrt{1-e^2}}{1-e^2\mu^2}\sin\omega(\sqrt{1-\mu^2}K_a\cos\alpha-\mu\sqrt{1-e^2}K_b\cos\omega\sin\alpha)-K_b\sin\omega\cos\omega\sin\alpha
\end{aligned}\right\} \quad (11)$$

These equations may be rewritten more simply by setting

$$F=\sqrt{1-\mu^2}\cos\alpha-\mu\sqrt{1-e^2}\cos\omega\sin\alpha$$

$$F_1=\sqrt{1-\mu^2}\sin\alpha+\mu\sqrt{1-e^2}\cos\omega\cos\alpha$$

$$H=\sqrt{1-\mu^2}\,K_a\cos\alpha-\mu\sqrt{1-e^2}\,K_b\cos\omega\sin\alpha$$

$$G=1-e^2\mu^2$$

$$F_2=\mu\sqrt{1-e^2}\sin\omega$$

Then

$$\left.\begin{aligned}
\frac{u}{U}&=\frac{FH}{G}+K_b\sin^2\omega\sin^2\alpha\\[4pt]
\frac{v}{U}&=-\frac{F_1H}{G}+K_b\sin^2\omega\cos\alpha\sin\alpha\\[4pt]
\frac{w}{U}&=-\frac{F_2H}{G}-K_b\sin\omega\cos\omega\sin\alpha
\end{aligned}\right\} \qquad (12)$$

The method of correcting for compressibility discussed in the text can now be approximately applied by increasing the fineness ratio by $1/\beta$ and reducing the tangent of the angle of attack by the factor β. Thus,

$$e_{st}=\sqrt{1-\frac{\beta^2}{f^2}} \qquad (13)$$

and

$$\tan\alpha_{st}=\beta\tan\alpha \qquad (14)$$

where e_{st} and α_{st} are the eccentricity and the angle of attack of the stretched body. Although this stretched body differs slightly from the properly stretched body, the approximation is very close for large fineness ratios and small angles of attack. It may be shown that the properly stretched body is an ellipsoid having three unequal axes; however, under the present restrictions the two minor axes are very nearly equal, so that only small errors will be caused by the above approximation of the stretched body.

The induced velocities in compressible flow are now determined by substituting α_{st} and e_{st} in equations (11) and multiplying the resulting velocity increments $\frac{u}{U}-1$, $\frac{v}{U}$, and $\frac{w}{U}$ by the factors $1/\beta^2$, $1/\beta$, and $1/\beta$, respectively, or

$$\left.\begin{aligned}
\left(\frac{u}{U}\right)_c&=1+\frac{1}{\beta^2}\left[\left(\frac{u}{U}\right)_{st}-1\right]\\[4pt]
\left(\frac{v}{U}\right)_c&=\frac{1}{\beta}\left(\frac{v}{U}\right)_{st}\\[4pt]
\left(\frac{w}{U}\right)_c&=\frac{1}{\beta}\left(\frac{w}{U}\right)_{st}
\end{aligned}\right\} \qquad (15)$$

The pressure coefficients for compressible flow may be computed from the velocities by the following formula:

$$P_c=\frac{\left\{1+\frac{\gamma-1}{2}M_0^2\left[1-\left(\frac{V}{U}\right)_c^2\right]\right\}^{\frac{\gamma}{\gamma-1}}-1}{\frac{\gamma}{2}M_0^2}$$

where

$$\left(\frac{V}{U}\right)_c^2=\left(\frac{u}{U}\right)_c^2+\left(\frac{v}{U}\right)_c^2+\left(\frac{w}{U}\right)_c^2 \qquad (16)$$

Combination of equations (12), (15), and (16) yields

$$1-\frac{V^2}{U^2}=\frac{1}{\beta^2}\left\{1-\frac{H_{st}^2}{G_{st}^2}-K_{b_{st}}^2\sin^2\omega\sin^2\alpha_{st}-\right.$$
$$\left(\frac{1}{\beta^2}-1\right)\left[\left(1-\frac{H_{st}F_{st}}{G_{st}}\right)^2+\left(K_{b_{st}}\sin^2\omega\sin^2\alpha_{st}+\frac{H_{st}F_{st}}{G_{st}}\right)^2-\right.$$
$$\left.\left.\left(\frac{H_{st}F_{st}}{G_{st}}\right)^2-2K_{b_{st}}\sin^2\omega\sin^2\alpha_{st}\right]\right\} \qquad (17)$$

where the subscript st is used to indicate that the various functions so identified are based on the values of e and α associated with the stretched body. (See eqs. (13) and (14).) A simpler first approximation may be obtained by considering the approximate relation

$$P_c=-2\left(\frac{u-U}{U}\right)_c$$

Since

$$\left(\frac{u-U}{U}\right)_c=\frac{1}{\beta^2}\left[\left(\frac{u}{U}\right)_{st}-1\right]$$

$$P_c=-\frac{2}{\beta^2}\left(\frac{H_{st}F_{st}}{G_{st}}-1+K_{b_{st}}\sin^2\omega\sin^2\alpha_{st}\right) \qquad (18)$$

A simpler equation may be developed for the pressures over a prolate spheroid at zero angle of attack by considering the method of approximate source-sink distributions described in references 2 to 4. In these references, it is shown that

$$P_c=-2\left(\frac{u-U}{U}\right)_c=\frac{1}{2\pi}\int_0^l\frac{S'(t)(x-t)dt}{[(x-t)^2+\beta^2r^2]^{3/2}} \qquad (19)$$

where t is a coordinate along the major axis of the body and $S'(t)$ is the derivative of the cross-sectional area of the body with respect to t. For a prolate spheroid,

$$S(t)=\pi r^2=\frac{4\pi b^2 t}{l}-\frac{4\pi b^2 t^2}{l^2}$$

from which

$$S'(t)=\frac{d[S(t)]}{dt}=\frac{4\pi b^2}{l}\left(1-\frac{2t}{l}\right)$$

Thus

$$P_c=\frac{2b^2}{l}\int_0^l\frac{\left(1-\frac{2t}{l}\right)(x-t)\,dt}{[(x-t)^2+\beta^2r^2]^{3/2}}$$

After integration and collection of terms

$$P_c=\frac{1}{f^2}\left[\frac{1}{2\sqrt{\left(1-\frac{x}{l}\right)^2+\beta^2\frac{r^2}{l^2}}}+\frac{1}{2\sqrt{\frac{x^2}{l^2}+\beta^2\frac{r^2}{l^2}}}-\right.$$

$$\left.\log\frac{1-\frac{x}{l}+\sqrt{\left(1-\frac{x}{l}\right)^2+\beta^2\frac{r^2}{l^2}}}{-\frac{x}{l}+\sqrt{\frac{x^2}{l^2}+\beta^2\frac{r^2}{l^2}}}\right] \qquad (20)$$

APPENDIX B

REDUCTION OF PRESSURE-COEFFICIENT FORMULAS TO OBTAIN SIMPLE FUNCTIONS FOR CORRECTING INCOMPRESSIBLE PRESSURE DISTRIBUTIONS FOR THE EFFECTS OF COMPRESSIBILITY

Two functions which may be used to express the relation between the pressure coefficients in compressible and incompressible flow are the ratio and the increment between the two coefficients P_c and P_i; that is, P_c/P_i and P_c-P_i. Both functions may be expressed in simple equations by substituting the pressure-coefficient functions for the midpoint of the body into both the ratio function and the increment function. In order to simplify equation (17) let $\mu=0$, $\sin \alpha_{si}=\beta\alpha$, and $K_{a_{si}}=1-k_{si}$ or $k_{si}=1-K_{a_{si}}$. Then,

$$1-\frac{V^2}{U^2}=\frac{1}{\beta^2}\left[2k_{si}-\frac{k_{si}^2}{\beta^2}-K_{b_{si}}\alpha^2(1-\beta^2)(K_{b_{si}}\beta^2\alpha^2-2k_{si})\right] \quad (21)$$

For small values of $1-\dfrac{V^2}{U^2}$

$$P_c=1-\frac{V^2}{U^2}$$

Also, for large values of f

$$K_{b_{si}}\rightarrow 2$$

Hence

$$P_c=\frac{1}{\beta^2}\left[2k_{si}-\frac{k_{si}^2}{\beta^2}-4\alpha^2(1-\beta^2)(\beta^2\alpha^2-k_{si})\right]$$

Since $\beta^2=1$ at $M_0=0$

$$\frac{P_c}{P_i}=\frac{1}{\beta^2}\frac{\left[2k_{si}-\dfrac{k_{si}^2}{\beta^2}-4\alpha^2(1-\beta^2)(\beta^2\alpha^2-k_{si})\right]}{2k_i-k_i^2}$$

Since $4\alpha^2(1-\beta^2)(\beta^2\alpha^2-k_{si})$ is small compared with $2k_{si}$, the term containing α may be neglected; thus

$$\frac{P_c}{P_i}=\frac{1}{\beta^2}\frac{k_{si}}{k_i}\frac{2-\dfrac{k_{si}}{\beta^2}}{2-k_i} \quad (22)$$

In order to reduce this equation to previously published forms (refs. 4 and 8), it is necessary to reduce k:

$$k=1-K_a=\frac{\log\left(\dfrac{1+e}{1-e}\right)-2e}{\log\left(\dfrac{1+e}{1-e}\right)-\dfrac{2e}{1-e^2}}$$

Substituting $e_{si}^2=1-\dfrac{\beta^2}{f^2}$ and the approximate form $e_{si}=1-\dfrac{\beta^2}{2f^2}$ in this equation gives

$$k_{si}=\frac{\beta^2(\log 2f-\log \beta-1)}{\beta^2\log 2f-\beta^2\log \beta-f^2} \quad (23)$$

and

$$k_i=\frac{\log 2f-1}{\log 2f-f^2} \quad (24)$$

These equations show that both k_{si}/β^2 and k_i are of order of magnitude $1/f^2$ and, therefore, small with respect to 2. Hence, the approximation (see eq. (22))

$$\frac{P_c}{P_i}=\frac{1}{\beta^2}\frac{k_{si}}{k_i} \quad (25)$$

is valid.

If equations (23) and (24) are used in equation (25), the following equation is obtained:

$$\frac{P_c}{P_i}=\left(1+\frac{\log \beta}{1-\log 2f}\right)\left[\frac{f^2-\log 2f}{f^2-\beta^2(\log 2f-\log \beta)}\right] \quad (26)$$

or for large fineness ratios

$$\frac{P_c}{P_i}=1+\frac{\log \beta}{1-\log 2f} \quad (27)$$

which may be changed to its equivalent form

$$P_c-P_i=\frac{2\log \beta}{f^2} \quad (28)$$

Equation (20) obtained by the source-sink-distribution method will also reduce to equations (27) and (28) for the central part of the body.

REFERENCES

1. Lees, Lester: A Discussion of the Application of the Prandtl-Glauert Method to Subsonic Compressible Flow Over a Slender Body of Revolution. NACA TN 1127, 1946.
2. Laitone, E. V.: The Subsonic Flow About a Body of Revolution. Quarterly Appl. Math., vol. V, no. 2, July 1947, pp. 227–231.
3. Laitone, E. V.: The Subsonic and Supersonic Flow Fields of Slender Bodies. Proc. of Sixth Inst. Cong. Appl. Mech., Sept. 1946.
4. Laitone, E. V.: The Linearized Subsonic and Supersonic Flow About Inclined Slender Bodies of Revolution. Jour. Aero. Sci., vol. 14, no. 11, Nov. 1947, pp. 631–642.
5. Munk, Max M.: Fluid Mechanics, Pt. II. Ellipsoids of Revolution. Vol. I of Aerodynamic Theory, div. C, ch. VII, secs. 2–9, W. F. Durand, ed., Julius Springer (Berlin), 1934, pp. 277–288.
6. Herriot, John G.: Blockage Corrections for Three-Dimensional-Flow Closed-Throat Wind Tunnels, With Consideration of the Effect of Compressibility. NACA Rep. 995, 1950. (Supersedes NACA RM A7B28.)
7. Hess, Robert V., and Gardner, Clifford S.: Study by the Prandtl-Glauert Method of Compressibility Effects and Critical Mach Number for Ellipsoids of Various Aspect Ratios and Thickness Ratios. NACA TN 1792, 1949.
8. Schmieden, C., and Kawalki, K. H.: Einfluss der Kompressibilität bei rotationssymmetrischer Umströmung eines Ellipsoids. Forschungsbericht Nr. 1633, Deutsche Luftfahrtforschung, 1942. (See also NACA TM 1233, 1949.)
9. Reissner, Eric: On Compressibility Corrections for Subsonic Flow Over Bodies of Revolution. NACA TN 1815, 1949.
10. Von Kármán, Th.: Compressibility Effects in Aerodynamics. Jour. Aero. Sci., vol. 8, no. 9, July 1941, pp. 337–356.